BEHAVIOR OF BULK SOLID MATERIALS SUBJECT TO VERTICAL VIBRATION IN STORAGE BINS

A Thesis Presented to the Faculty of
Graduate Studies of the University of Manitoba

By

Tun Ge

In Partial Fulfilment of the Requirements for the Degree of Doctor of Philosophy

Department of Biosystems Engineering
University of Manitoba
Winnipeg, Manitoba

THE UNIVERSITY OF MANITOBA

FACULTY OF GRADUATE STUDIES

*****

COPYRIGHT PERMISSION PAGE

BEHAVIOR OF BULK SOLID MATERIALS SUBJECT TO VERTICAL VIBRATION IN STORAGE BINS

BY

TUN GE

A Thesis/Practicum submitted to the Faculty of Graduate Studies of The University of Manitoba in partial fulfillment of the requirements of the degree of

Doctor of Philosophy

ABSTRACT

The behavior of bulk material storage systems (bins and silos) subject to low-amplitude vibration was studied through model simulations and experiments. In the simulation models, the bulk solids were discretized into layers, and the normal contacting forces were represented by springs and the internal friction (dissipative) forces were represented by dampers. In the first phase of the study, the models were applied to the prediction of material consolidation in grain storage bins subjected to low-amplitude vibration. It was hypothesized that grain consolidation was a result of grain kernels being ushed into the adjacent layers by the inertial force during vibration (the wedge-in hypothesis). The Lagrange equation was applied to the kinetic energy, the elastic energy, and the friction equivalent dissipation function for each layer of the grain mass. The vibration equations were then derived for the grain system. The consolidation between two adjacent layers was calculated from the difference between the vibration amplitudes of the two layers. To validate the consolidation model, a model bin 150 mm in diameter and 292 mm in height was used to collect experimental data. The bin was filled with wheat which had an initial bulk density of 798 kg/m^3, kernel density 1439 kg/m^3, and internal friction angle 25°. The bin was subjected to vibration at frequencies of 23, 30, and 48 Hz. For each frequency, the vibration amplitude was increased from 0.011 to 2.22 mm in 15 increments. At each amplitude increment, the bin was allowed to vibrate until no further settlement could be observed (about 5 minutes) and the grain settlement was measured using a ruler and level at more than four locations. The predicted consolidation compared favorably with the experiment data. It was found that the maximum consolidation was independent of the vibration frequency. However, the higher the frequency, the lower the amplitude at which maximum consolidation occurred.

During vibration, bulk solids consolidate vertically and tend to expand laterally becuae particles re-orient. The tendency of lateral expansion and particle re-orientation may cause the pressure on the bin walls to increase. Based on the wedge-in hypothesis, a theoretical formula was derived for predicting the vibration-induced (dynamic) pressure on the bin walls. The dynamic pressure was derived as the resultant of two components: the pressure increase induced by the changes in particle contacts and the pressure increase caused by the tendency of lateral

expansion. The calculated dynamic pressures were in good agreement with the measured data reported in the literature.

The second phase of this study dealt with arching problems in storage systems for cohesive bulk solids. A theory was developed to explain the mechanisms of arch formation and destruction during vibration. In this theory, the force equilibrium condition on an arch was considered. It was hypothesized that an arch would collapse during vibration when the self weight of the arch and the inertia force caused by vibration exceeded the shear forces acting on the arch. It was proven that an optimal frequency for arch destruction had to satisfy two conditions: (1) it had to be one of the natural frequencies of the bulk solids system so that a prominent amplitude peak would appear during vibration, and (2) its peak of vibration shape in should appear at or close to the arch location. If these two conditions were satisfied, the least vibration energy was required to destruct arches. The theory also showed that not all natural frequencies were suitable for destructing arches. To evaluate the natural frequencies of bulk solids systems, an inverse superposing algorithm was derived. A series of experiments were performed to validate the theoretical models. For a model storage bin filled with cohesive feed, 33 and 90 Hz were measured to be optimal frequencies for destructing the arches. The predicted optimal frequencies were 34.4 and 94.8 Hz. The differences between the theoretical and measured optimal frequencies were less than 6%.

ACKNOWLEDGMENTS

I take this opportunity to sincerely thank my supervisor, Dr. Q. Zhang for his invaluable guidance and encouragement throughout the course of this project. His positive attitude and words of comfort always inspired me to a further success.

I am indebted to Dr. M. G. Britton who also gives me a lot of guidance and help in my research. And his review and suggestions for my thesis is valuable.

I am very grateful to Dr. Arvind H. Shah for his serving on my advisory committee and his review and suggestion for my thesis.

I am thankful to Dale Bourns, Matt McDonald, Jack Putman, and Gerry Wood who helped me in building the experimental device, installing computers, repairing equipment for my experiment and giving advices on utilizing of departmental facilities.

I wish to give thanks to Natural Science and Engineering Research Council of Canada (NSERC) for funding this project. I appreciate the research assistantship, and the fellowships from the University of Manitoba, Faculty of Engineering, and Department of Biosystems Engineering.

I am extremely grateful to my parents for their continuous encouragement and great support throughout my entire education.

I lack words of gratitude for my wife Lixin Wang and my daughter Zhan Ge, whose love and affection always gives me strength to overcome difficulties one by one.

TABLE OF CONTENTS

LIST OF TABLES

LIST OF FIGURES

Chapter 1. INTRODUCTION

It was well known from the engineering practice that bulk solids storage and handling systems are subject to a much higher rate of failure than other structural systems. These failures can be classified in two categories:

(1) structural failures, such as denting, collapsing, and foundation failures.

(2) functional failures, such as arching, ratholing, flooding, segregation, attrition implosion, caking, and non-uniform blending.

In structural design, the load exerted by the stored bulk solids is one of the most important factors which determine whether a storage bin is strong enough to hold the bulk solids. Drescher (1991) indicated that redistribution of stresses within the bulk material took place upon the opening of the outlet. This stress redistribution, commonly known as discharge loading, could significantly impact the magnitude and distribution of wall stresses. Numerous experiments on full scale and model storage structures have revealed that hazardous level of bin wall stresses could occur during discharge. This discharge load becomes even more critical when the discharging outlet is eccentrically arranged.

The properties and behavior of bulk solids directly affect the processing and conveying of bulk solid materials. For example, the poor flow behavior will cause severe problems such as arching and piping in the conveying of bulk materials in processing plants. Flow problems have long been a challenge to many researchers and design engineers. As early as in 1964, Jenike, based on his and his co-worker's pioneering research, elucidated an initial analysis method to deal with the behavior of bulk solids and to design bulk solid storage vessels systematically.

The difficulties in dealing with bulk solids flow are:

(1) complex behavior of bulk solids in loading, and flowing (bulk solids consist of solid particles and voids and their properties change with the operation conditions in handling facilities),

(2) interactions between bulk solids and their surroundings,

(3) high cost in running full-scale tests, and

(4) the field is not widely recognized at the university level.

Early in the 70's, Myers (1970), Suzuki et al. (1972), Carroll et al. (1975), Roberts et al. (1978, 1986)

and many other researchers explored the effects of vibration on the bulk solids flow, and tried to use vibration as a possible solution to the flow problems of bulk solids. But their effect were not quite successful in industrial application because the behavior of bulk solids under vibration are not fully understood. Different bulk solid materials react totally differently to the same vibration condition. Even the same material stored in different conditions will exhibit a different behavior to a certain vibration condition.

Under vibratory condition, a bulk solid behaves like a system with multi-degrees of freedom and it can be modeled into a series of layers. Each layer of the bulk solid has a mass and all layers are interactively connected with contacting forces and internal dissipation forces. The motions of these layer are governed by the mass, contacting forces and dissipation forces. The natural frequency and the vibration shape change with many factors, such as the amount of the bulk solids and the properties of the bulk solids. At some frequencies, the vibration exerts a positive effect on flowability if the peak amplitude occurs at an arch layer. At other frequencies, the vibration causes serious consolidation in the mass making flow more difficult when the arch layer happens to be at a vibration node.

To date, few theories have been advanced to quantitatively describe the effect of vibration on the flow behavior of bulk solids. Some vibrators that are presently used in the industry, including the pneumatic powered (reciprocating air-cushioned piston) drives, the electromagnetic drives, and dual rotary electric vibrators usually have one or more predetermined frequencies. These frequencies may not supply the most suitable vibration for flow improvement. Therefore, these vibratory devices may not deliver satisfactory solutions to flow problems. Some may even have negative effects if not used properly.

This research established a quantitative mathematical model to simulate the behavior of bulk solids during vibration. The consolidation of the bulk solid subject to vertical vibration and its effect on lateral pressure were studied. Analysis of the effect of different vibration patterns on the flowability of the cohesive bulk solids were conducted. A practical engineering approach for selecting the most suitable vibration conditions for preventing arching problems was developed.

Chapter 2. LITERATURE REVIEW

2.1 Bulk Solid Flow

There are two flow patterns existing in bulk solids storage bins during discharge. The first one is known as " mass flow". It is characterized by the following conditions: (1) the total volume of the stored material is in motion; (2) no channeling, hang-ups, surging and flooding; (3) first-in, first-out; (4) no dead regions; (5) good mixing; (6) uniform flow; (7) high dynamic pressures on the wall; and (8) high degree of wearing on the wall. The second flow pattern is known as "funnel flow", characterized by: (1) a portion of the stored material is in motion; (2) last-in, first-out; (3) consolidation of dead regions; (4) impact forces due to pipe collapses; (5) varying density; (6) size segregation; (7) possible flooding; and (8) less wearing on the wall.

For most industrial applications, the mass flow pattern is desired since it creates less flow problems than the other pattern, such as no channeling, hang-ups, surging and flooding. Janike and Leser (1964) found that the wall friction, the internal friction of the material and the half angle of the hopper contributed mostly to the formation of mass flow. Gaylord and Gaylord (1984) obtained a consistent conclusion with Jenike and Leser. They found that to obtain a mass flow, the hopper walls needed to be sufficiently steep and smooth. Jenike and Johanson (1969) found that a flow controlling device was also important in inducing mass flow.

Giunta (1969) studied the flow patterns of granular materials in flat-bottom bins. He developed a theory to predict the boundary of the flow patterns that occurred in these bins when circular openings were used. The theoretical work was based on the work by Johanson and Jenike (1962) on flow in a converging channel, with an assumption that a combination of radial and elementary stresses described the flowing mass in the active region. In the derived equation, the resultant flow pattern was a function of the effective angle of friction, the opening size, and the head of material in the bin.

Savage and Jeffrey (1981) presented a fluid mechanics-like theory to describe the flow of granular materials. They focused their analysis on the ratio R of the characteristic mean shear velocity to the particle fluctuation velocity. They applied their analysis to three different physical

situations; namely, (1) fluidized beads (R<<1), (2) dry granular flows (R≈1), and (3) Bagnold's granulo-viscous flow (R>>1). The weakness in their analysis is the inability to determine R. They indicated that it might be possible to determine R explicitly by establishing a balance between the input mechanical work and the energy dissipation in the sheared granular mass if considering the particles as rough, inelastic, and having finite rotary inertia. Their study showed that the level of agreement between the theory and experimental observations was encouraging.

2.2 Arch Formation and Prevention

There are two basic types of arching, namely mechanical and cohesive arching in bulk solid systems (Shamlou 1988). Mechanical arching occurs when the opening of the outlet is a few times greater than the maximum particle size of the stored material. For large free-flowing particles, they easily interlock to block the outlet of a hopper. Cohesive arching happens when the stored material develops a strength strong enough to support an obstruction to flow. Cohesive arching is usually a more important issue to be concerned with because it is more difficult to predict. Shamlou (1988) described the mechanism of formation of cohesive arching in detail. In the worst scenario, there is no force acting on either upper or lower boundaries of the arch, and the only force which may destroy the arch is the weight of the arch itself (fig. 2-1). Thus at any section of the arch, the minor principal stress is zero, in the direction normal to the free surface, and the major principal stress is tangent to the free surface of the arch. The arch can be broken only in the case when the major principal stress σ_1 reaches the unconfined yield strength f_c of the stored material. For cohesive materials, f_c increases with the consolidation pressure σ_c, moisture content, temperature, and time of consolidation (Jenike, 1964). Mathematically,

$$f_c = F(\sigma_c)(t, m_c, T, \cdots) \tag{2-1}$$

where:

f_c = unconfined yield strength of solid (Pa),

F( ) = flow function,

σ_c = consolidation pressure (Pa),

t = time of consolidation at rest (s),

m_c = moisture content (%), and

T = temperature (C).

During continuous flow, moisture content and temperature are usually taken as a constant. When the time of consolidation equals zero, f_c is usually considered to be a function of consolidation pressure only.

The flowability of cohesive materials is measured primarily by the flow function. From the force equilibrium, Jenike (1964) derived the following equations to predict the minimum opening that will prevent arching.

$$B = \frac{f_c}{g\gamma} \tag{2-2}$$

for wedge-shaped bins, and

$$D = \frac{2f_c}{g\gamma} \tag{2-3}$$

for the minimum diameter of a circular opening in conical bins.

where:

B = minimum width of a rectangular opening to prevent arching (m),

g = gravitational acceleration (m/s^2),

γ = bulk density of solid (kg/m^3), and

D = minimum diameter of a circular opening that prevents arching (m).

Drescher et al. (1995) discussed the arching theory in symmetrical hoppers. They analyzed and compared the existing structural mechanics-based theories and the continuum mechanics-based theories. In the former theories, the effective yield locus must be taken as linear, passing through the origin of the σ_n-σ_t plot (σ_n is the normal stress, and σ_t is the shear stress), and the instantaneous yield locus should be non-self-similar. In the latter theory, any shape or self-similarity of instantaneous yield locus is acceptable as long as the effective yield locus becomes linear and passes above the origin of the σ_n - σ_t plot. Their tests indicated that experimental results often deviated from the

required pattern. They mentioned a concept of a curved and convex effective yield locus passing through the origin of the σ_n - σ_t plot. They also discussed another possibility of relaxing the constraints imposed on the flow function. That is to assume that the consolidating stresses in the hopper satisfy not the effective yield condition, but another function mathematically similar to effective yield locus.

To improve the flowability of bulk solids, flow promoting devices may also be used. This option is especially practical and useful if the storage bin was not originally designed to operate under mass flow conditions. There are various kinds of flow promoting devices. The following is a list of examples:

(1) Air lance.

An air lance blows air into the material via a perforated piece of pipe located in the material close to the hopper opening. It was found that the best location for the air lance was about 4 times the diameter of the outlet above the opening (Williams et al, 1983).

(2) Air cannon.

It expels an explosive charge of compressed air directly into the hopper at the level where the blockage is expected. Rappen and Wright (1983) applied an air cannon to initiate air flow in bunkers.

(3) Insert.

An insert is a physical object placed in bins to help promote bulk solids flow. Physically, inserts can be a circular cylinder, a bar with triangular cross section, or a bar with rectangular cross section. Various kinds of specially designed inserts are used to act as flow correcting devices. Johanson (1966) derived a theory to predict the region influenced by the insert and following this theory he developed a procedure to predict the appropriate position for installing inserts to create mass flow in a bin. He indicated that the stagnant zones in a funnel flow bunker could be greatly reduced and the flow quality could be improved by selecting a suitable shaped insert and installing it at the critical height above the opening. Ersov and Lisin (1964) showed that the relative position of insert to the bin outlet is an important factor influencing the flowability of bulk solids. Too small

or too great distance between the outlet and the bottom of the conical inserts would make the flow quality worse. Kvapil and Tanaka (1965) found that the active flow region became larger when a horizontal baffle was placed over the bin opening. By calculation, they gave a minimum baffle dimension to improve the flow. Their further studies showed that large inserts near the junction of the bin and the hopper might help develop mass flow and the inserts near the bin outlet were beneficial in eliminating piping and arching. Neeraj (1998) studied the effects of insert location, size, surface friction, hopper outlet size, hopper slope, and bin wall friction on stress distribution in ground feed stored in bins by applying the modified Cam-clay model. In his study, a commercial software SIGMA/W was used to prepare models of storage bins and solve finite element equations. He concluded that flowability increased and then remained unchanged as the insert was mounted higher up in the bin. Also flowability increased as the insert size and friction was decreased. Flowability increased with increased hopper outlet size but decreased as hopper slope was reduced.

(4) Vibrators.

As a flow promotion method, mechanical vibration may be applied in several ways. In some cases, vertical vibration may be appropriate and in other cases the vibration may be applied in the horizontal direction or more generally in an oblique plane. Roberts et al (1979) pointed out that an important fact was the manner in which the vibration energy was transmitted through the material mass. It should be transmitted in a way that would ensure a reduction in shear strength in the critical regions of the flow obstruction. Arnold et al. (1977) illustrated the effect of vibration on the consolidation strength of bulk solids by applying a Jenike shear cell fitted with a vibration exciter. It was clearly shown that the application of mechanical vibration can significantly reduce the frictional drag against a hopper wall. In an experimental study, Roberts and Scott (1978) found that the strength and the corresponding flow function of bulk solids were frequency dependent, and there were some particular frequencies at which the shear strength and flow functions become minimum. Also Roberts et al. (1986) indicated that the shear strength of bulk solids decreased exponentially with the increase in the vibration velocity until the limiting critical state condition was obtained.

2.3 Discharge and Vibration Loads in Bulk Solids Storage Structures

Discharge loads are dynamic loads which are induced during the emptying process of the bins. When the bulk solid material is discharged from the bin, it can increase the loads on the bin walls considerably.

Jenike et al. (1973), Walker and Blanchard (1967), Moriyama and Jotaki (1980) confirmed that a wall pressure reduction occured in the lower regions of a hopper during flow, while wall pressure was found to increase substantially in a localized region near the transition from hopper-to-bin. These results suggested an equilibrium consequence of a switch in pressure fields at the transition from an active to a passive stress field.

Richard and Elwi (1990) developed a finite element model to analyze incipient flow for cohesionless material in silos. They simulated initial filling and opening of the outlet (the initiation of incipient flow). They found the switch pressure obtained at the outlet was greater than the static pressure, but smaller than those obtained using Jenike's and Walker's solution (Janike et al., 1973; Walker et al., 1967). They suggested that the switch point had a finite thickness, and distribution of the unbalanced load over this thickness was the cause of reduced wall pressures. Finally they concluded the design pressures could be in between static pressure that is not localized, and those pressures predicted by Jenike et al. (1973) and Walker et al. (1967) that are highly localized.

Xu et al. (1993) studied the dilation phenomenon of bulk grain. They indicated that when grain flows to the discharge outlet vertical shearing occurs because of the relative movement within the grain mass. The shear deformation can be analogized as sliding between two serrated faces of rigid blocks. And thus when it happens it will cause a horizontal dilation (volume increases) within the grain mass. This dilation is characterized by the angle of dilatancy. This dilation theory was adopted to explain discharge loads that occurred in storage structures for bulk solids.

For the discharge loads, there are two other hypotheses, i.e., (1) switch theory (Jenike and Johanson, 1969) and (2) impact theory (Kmita, 1991; ACI, 1983) besides the dilation theory proposed by Smith and Lohnes (1980). Xu et al. (1993) pointed out that among the above three hypotheses for discharge loads, dilation theory is the only one which considers the effect of the

stored materials on dynamic loads. They established a mechanical model and derived the following equations for discharge loads:

$$P_d = \frac{P}{2\tan(\frac{\pi}{4} - \frac{\gamma}{2})} \tag{2-4}$$

$$f = \frac{P_d}{P_S} = \frac{1}{2k\tan(\frac{\pi}{4} - \frac{\gamma}{2})} \tag{2-5}$$

Where:

P_d = discharge load (N),

P = weight of a typical central moving block of the bulk solids (N),

γ = angle of dilatancy (radians),

f = over pressure factor,

P_S = static lateral force (N), and

k = ratio of lateral force to vertical force.

They validated their model with experimental data. Their sample calculations suggested that the over pressure factors in various design standards and codes could be estimated from the dilatancy angle.

Hao et al. (1992) carried out an experiment in which a grain bin 1.0 m in diameter and1.5m in height was subjected to vertical vibration. They found that the grain bulk density increased 5% and the grain depth decreased 3% after 20 minutes of vibration. They also measured an increase of 39% in lateral pressure near the bin bottom (0.15m from bin bottom). They indicated that according to Janssen's theory, a 5% increase in the bulk density would result in a 5% increase in lateral pressure at all depths, whereas a 3% decrease in grain depth would cause a 19% decrease in lateral pressure at the top level and 3% at the bottom level. Therefore, the net change in lateral pressure

should be a decrease of 14% at the top level and an increase of 2% at the bottom level. This calculation did not agree with the measurements. Hao et al.(1992) pointed out that there must be some other contributing factors besides the density change. They explained that lateral expansion was responsible for the large increase in lateral pressure after the bin was vibrated.

2.4 Numerical Methods for Studying the Behavior of Bulk Solids System

Owing to the discontinuity characteristics of the bulk solid system, the conventional analytical methods are usually no longer applicable. It is also very difficult to solve a complicated problem by analytical methods. With numerical methods, the bulk solid systems are discretized into small elements. With the development of the computer, the numerical methods become more and more effective in solving the problems involved in bulk solid systems. The most widely used numerical methods in bulk solid systems are the finite element method and the discrete element method.

Yoshida (1996) carried out a numerical study by applying a three-dimensional distinct element method (3-D DEM) to simulate the vertical vibration of the particles in a bin. The mechanism of particle convection was investigated in detail by considering the behavior of individual particles. The numerical simulation modeled a bin with 16.5 mm in diameter and 27 mm in height. A total of 6000 particles of 1 mm diameter were used in the simulation. At first, the particles were distributed in the cylindrical space at random and the gravitational force was applied. It took 10000 iterations in the simulation to reach the convergence of the particle movement. The locus of any particular particle was traced in the entire time domain for the whole material mass. From the simulation, a hill-like shape of the surface was found to be formed by particle convection. The velocity of downward movement was found to be the fastest along the wall, and the upward movement near the center appeared to be the fastest.

Rong et al. (1995) developed a numerical model by utilizing the discrete element method to simulate the mechanical behavior of a bulk solid material consisting of uniform, inelastic, frictional and deformable discs. They employed an explicit time difference scheme in which each calculation cycle included the application of two simple force displacement laws at all contacts. Their model

kept track of the motion of individual particles and updated any contacts with neighboring particles during discharge. For particle motion, the dynamic equation of equilibrium was adopted as the governing equation:

$$m\ddot{r}_i + C\dot{r}_i + Kr_i = F_i \qquad (2\text{-}6)$$

where

m = particle mass (kg),

C = damping coefficient,

K = stiffness (N/m),

F_i = externally applied force on particle i (N), and

$\ddot{r}_i$, $\dot{r}_i$, r_i = acceleration, velocity, and displacement of the particle respectively (m/s^2, m/s, m).

A good agreement was found between the calculated trajectories and experimental measurement of individual particles in the 195 particle, and 750 particle simulations. They indicated that in general, the particles with a rougher surface moved more slowly than the particles with a smoother surface. Their numerical simulation of granular flow also showed that the horizontal velocity of particles increased from almost zero at the centerline to two symmetrical maxima at about one-third the distance to the wall and then decreased toward the walls. While the vertical velocity varied from a maximum value at the centerline to a minimum near the walls. In the flow behavior analysis for idealized particles (discs), Rong et al. (1995) focused on two distinct aspects: occurrences of shear bands and use of flow corrective inserts. Two series of numerical simulation were performed with model bins of various shapes in their study. And it was found that shear bands developed in the hopper at the same moment as flow initiates. These shear bands swiftly moved upward into the vertical part of the bin. The simulation and experimental observation showed that fewer shear bands tend to occur in materials with a high coefficient of interparticle friction while a more intense shear band phenomenon was found in materials with a high coefficient of restitution. Comparison of

simulations between solid and hollow particles indicated that a higher density could cause a more intense shear band during flow. They concluded that to maintain a discharge rate similar to unobstructed flow the corrective insert should be placed at an optimum height above the bin outlet and its size should be at least five times the particle diameter. The flow pattern investigation showed that voids and velocity discontinuities appeared during emptying of the bin. At the transition zone from parallel flow to convergent flow, the velocity changed abruptly and was accompanied by particle rotations.

Meng et al. (1997) utilized a secant constitutive relationship in a transient finite element analysis of stresses, displacements and velocities in the solids during discharge of a silo filled with soybeans. In their research, the stresses and strains are related by a secant relationship that has an elastic and a plastic component:

$$\{\sigma\} = [D^{ep}]\{\varepsilon\} - \{\sigma^{p}\} \tag{2-7}$$

where:

$\{\sigma\}$ = stress vector,

$\{\varepsilon\}$= strain vector,

$[D^{ep}]$ = an introduced elastic matrix, and

$\{\sigma^{p}\}$ = a plastic stress vector.

All the material parameters in this constitutive relationship were determined in their experiment. They used a model silo with a hopper to verify the numerical result. The silo had a length to width ratio of about 3 to approximate a plane strain situation. The particulate material used in the experiment was soybeans. The vertical bending strains in the silo wall were measured with strain gauges. The experiments were conducted with hopper openings of 40, 60, and 80 mm widths over the entire opening length. The straight part of the hopper has a dimension of 1.25m×0.4m×1.2m in length , width, and height respectively. The height of the lower part of the hopper is 0.56m. Their research results showed that the finite element analysis was capable of predicting wall pressures during entire the period of discharging. The analysis procedure was stable. Furthermore they found it was relatively easy to determine the parameters in the constitutive relations by experiment.

In the subsequent parametric study, Meng et al. (1997) found a consistent result of normal wall pressure with Janssen's theory. That is, the normal wall pressure was significantly smaller for larger wall friction coefficient. The highest normal wall pressure was found at the location where the bin cylinder met the hopper. The parametric study also showed that the friction between the wall and soybean and the hopper opening had a significant effect on normal wall pressure. In the hopper zone, the normal wall pressure increased considerably beyond the static pressure in the first few seconds of flow. But in the cylinder zone, it increased very little. They confirmed a phenomenon that had been predicted and described by many other researchers. That is, in the hopper zone, the direction of major principal stress gradually changes from vertical to horizontal when the bulk solids begin to flow out.

Lu et al. (1997) combined the finite element method (FEM) and the discrete element method (DEM) to develop a hybrid numerical model. The main idea was that in most regions inside the bins, the FEM is accurate enough to simulate the movement of particulate solids as a continuum. But in certain regions, such as in the lower part of a hopper near the outlet and in the regions where there are large shear deformations such as at the intersection of a vertical wall and an oblique hopper wall, the continuum model for bulk solids was no longer accurate and the DEM would be the preferred procedure. In proceeding with this approach, they made the following assumptions: (1) the granular material consisted of assembly of round particles of the same size and shape, and the diameter was assumed to be much larger than the distance between particles; (2) the material was cohesionless; (3) only the elastic deformation of individual particles was considered in the DEM. Plastic deformations of individual particles are negligible; and (4) the movement of particles was restricted to two dimensions.

To link the FEM and DEM models at the interfaces, the displacements at the interfaces were obtained from FEM analysis, and these displacements were used as the boundary conditions for the DEM.

To validate this hybrid model, measured data from Negi et al. (1997) was used to performed a statistical analysis to verify the degree of agreement between the experimental and numerical

results of wall pressures. They found that the values predicted by the numerical model lie within the 95% confidence interval.

After this hybrid model was validated, Jofriet et al. (1997) used it to solve bulk solid flow problems for 7 symmetric bins with varying wall frictions, hopper slopes and discharge openings and for 4 asymmetric bins with varying wall friction only. Their results showed that: (1) the friction between the stored material and bin wall was the most important factor affecting wall pressures throughout the bin. The lower the friction, the larger the lateral wall pressure, and the higher the discharging velocity; (2) the over-pressure at the flow constriction caused by a hopper was affected by the flow velocity; (3) an increase in the hopper angle caused a decrease in discharge velocity and an increase in normal wall pressure at the junction of the vertical wall and hopper. This increase was due principally to gravity force on the hopper wall surface that was less steep; (4) for an asymmetric hopper, a mirror over pressure phenomenon occurred along the straight wall at the level where the hopper caused a flow constriction.

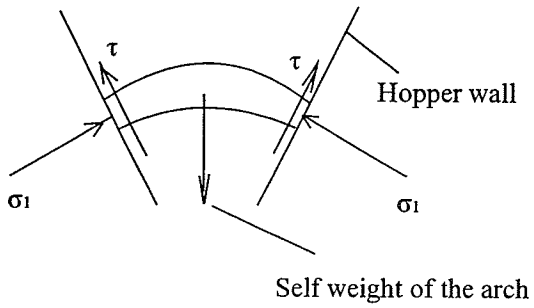

Figure 2-1. Diagram of the worst scenario of arch destruction

Chapter 3. OBJECTIVES

Vibration causes changes in the spacial arrangement of particles in bulk solids. To date, however, few theories have been advanced to quantitatively describe the effect of vibration on the mechanical properties of bulk solids. Still less is known about the quantitative effect vibration has on preventing the formation of arches. There is a need to investigate the behavior of bulk materials under vibratory conditions to develop a feasible approach to applying vibration as an aid to solve arching problems in bulk solid storage systems.

The objectives of this research are to:

(1) develop numerical models for predicting the consolidation of bulk solids in storage bins when subjected to vibrations,

(2) investigate the increase in lateral pressure in the storage structures subjected to vertical vibrations,

(3) develop a mechanics model to simulate the vibration characteristics of bulk solid systems,

(4) derive an algorithm to solve the vibration modes and resonant frequencies numerically, and

(5) investigate the effects of these vibration characteristics on arch destruction and flowability in bulk solid systems.

Chapter 4. CONSOLIDATION OF GRAINS IN STORAGE BINS SUBJECTED TO VERTICAL VIBRATION

Summary

A theoretical model was developed to predict vibration induced grain consolidation (vertical settlement) in storage bins. In the theory, grain kernels were modeled as spheres connected by elastic springs and frictional dampers. Governing differential equations were then developed for this spring-damper system and solved numerically. It was hypothesized that grain consolidation resulted from grain kernels being "pushed" into the adjacent layers by the inertial force during vibration. An experiment was conducted to measure grain consolidation in a small model bin filled with wheat to validate the predictive model. The bin was subjected to vibration at frequencies of 23, 30 and 48 Hz and amplitudes up to 2.3 mm. The predicted grain consolidation compared favorably with the experimental data. It was found that the maximum consolidation (density) was independent of the vibration frequency. However, the higher the frequency, the lower the amplitude at which the maximum consolidation (density) occurred. Both the vibration amplitude and frequency affected the variation of grain consolidation with the grain depth.

4.1. Introduction

Storage structures for bulk solids are often subjected to low amplitude vibrations caused by routine operations, and train and vehicle traffic. Vibration is sometimes also induced purposely to shake loose the stored materials for flow improvement in bins. Because bulk solid materials consist of solid particles and air voids, vibration may change the spacial arrangement of the particles, and thus the bulk properties of the material such as bulk density, internal friction, and friction between the material and the structure may change. Roberts et al. (1986) conducted shear tests on cohesive powders subjected to vibration. They found that the shear strength was reduced significantly by the application of mechanical vibration, and so was the powder-bin wall friction. Xu et al. (1993) performed triaxial tests on bulk wheat and found that the strength (the maximum deviatoric stress) and dilatancy of bulk wheat increased after samples were vibrated. From the operational point of view, changes in bulk properties may cause severe structural and functional problems in the storage structures. Hao et al. (1994) reported that vibration of grain bins caused a 39% increase in lateral

pressures on the bin walls in a model bin filled with wheat. The objectives of this research were to: (1) develop a model to predict consolidation of grain in storage bins subjected to vertical vibration, (2) conduct an experiment to validate the predictive model, and (3) predict the effects of vibration frequency and amplitude on grain consolidation. It should be noted that this study dealt with low amplitude vibration which would cause changes in the spacial arrangement of particles in bulk solids systems, but not produce significant dynamic forces on the storage structures.

4.2 Model Development

It has been a well-known fact that vibration results in increased bulk densities of bulk solids. This means that bulk solids consolidate vertically and might expand laterally if allowed when they are subjected to vibration. A "wedge-in" mechanism is proposed herein to describe the consolidation of bulk solids under vertical vibration. If a bulk solid material is viewed as being layers of particles, the upper-layer particles "wedge" into the lower layer because of the "push" by vibrational (inertial) force, causing the vertical consolidation and lateral expansion (fig. 4-1). Vertical consolidation is indicated by the change in the thickness of the two layers (h_0 - h). To predict the consolidation caused by wedge-in, the following assumptions are made: (1) a bulk solid material consists of equal-sized spherical particles, (2) the material is subjected to vibration only in the vertical direction, (3) wall friction has negligible effect on vibrational motion of particles, and (4) all the particles in a horizontal layer are subjected to the same vibrational motion. Based on these assumptions, a pair of adjacent layers of bulk solid in a bin can be represented by three particles (fig. 4-1b) and a one-dimensional vibration model is proposed to represent all layers in the vertical direction (fig. 4-2). To derive the governing equations, a particle P_i in layer *i* at a depth of y_i from the bin bottom is considered. This particle rests on two particles in the lower layer (*i-1*) (fig. 4-1a). The horizontal clearance between the two particles of the lower layer is 2S and the structure angle (angle between the lines connecting P_i and P_{i-1} in the horizontal direction) is θ (fig. 4-1b). Contact forces acting on particle P_i are frictional and normal forces (fig. 4-2), and they are calculated as:

$$N_{di} = (\rho g)(Y_0 - y_i)\sin\theta \qquad (4\text{-}1)$$

$$F_{di} = (\tan\varphi)(\rho g)(Y_0 - y_i)\sin\theta$$
$$=(\rho g)(Y_0 - y_i)\tan(\varphi)\sin\theta \quad (4\text{-}2)$$

where:

θ = structure angle (°),

N_{di} = normal contact force (N),

F_{di} = frictional contact force (N),

φ = internal friction angle (°),

ρ = bulk density (kg/m^3),

g = acceleration due to gravity (m/s^2),

Y_0 = total depth of stored material (m), and

y_i = depth of the *i*th layer (m).

Dissipative friction between particles are modeled by dampers, while normal contacts between layers are assumed to be elastic and modeled as spring elements (fig. 4-2). The equivalent coefficient of friction damping is determined as follows (Beards, 1983):

$$c_d = 2\left(\frac{4F_{di}}{\pi\omega X_i}\right) \quad (4\text{-}3)$$

where:

c_d = equivalent viscous damping coefficient (N·s/m),

ω = angular frequency of exciting force (1/s), and

X_i = amplitude of vibration (m).

Kinetic energy of particle P_i during vibration is given as:

$$T_i = \frac{1}{2}m_i\dot{x}_i^2 \quad (4\text{-}4)$$

and the elastic energy is determined as:

$$V_i = 2\left(\frac{1}{2}\right)\left\{k([x_i - x_{i-1}]^2 + [x_{i+1} - x_i]^2)\right\}\sin^2\theta \quad (4\text{-}5)$$

where:

T_i = kinetic energy (N·m),

V_i = elastic energy (N·m),

m_i = particle mass (kg),

k = inter-layer stiffness (stiffness between the two adjacent layers) (N/m),

x_i = displacement of particle P_i (m) along line of contact forces,

x_{i-1} = displacement of particle P_{i-1} (layer below the *i*th layer) (m),

x_{i+1} = displacement of particle P_{i+1} (layer above the *i*th layer) (m), and

$\dot{x}_i$ = vibrational velocity of particle P_i (m/s).

For the layers at the free surface and the bin bottom, elastic energy is calculated differently because they are not adjacent to grain layers on one of the two sides:

$$V_1 = 2\{\frac{1}{2}k([x_1 - x_1]^2 + [x_{1+1} - x_1]^2)\}\sin^2\theta = k\sin^2\theta(x_2 - x_1)^2 \tag{4-6}$$

$$V_n = 2\{\frac{1}{2}k([x_n - x_{n-1}]^2 + [d_f - x_n]^2)\}\sin^2\theta \tag{4-7}$$

where:

V_1 and V_n = elastic energy for the top and bottom layers, receptively (N·m),

d_f = deflection of the bin-floor (m).

The friction equivalent dissipation function U_i is given as (Beards, 1983; Davies, 1980):

$$U_i = \frac{1}{2}c_d\dot{x}_i^2 \tag{4-8}$$

Applying Lagrange's equation to equations (4-4) to (4-8) yields (Davies, 1980):

$$\frac{d}{dt}\left(\frac{\partial T_i}{\partial \dot{x}_i}\right) - \frac{\partial T_i}{\partial x_i} + \frac{\partial V_i}{\partial x_i} + \frac{\partial U_i}{\partial \dot{x}_i} = F_{xi} \tag{4-9}$$

where:

F_{xi} = external force applied on particle P_i in the vertical direction due to grain mass above it in bin(N)

Substituting equations (4- 4), (4-5), and (4-8) into (4-9), the following vibration equation is obtained for the *i*th layer:

$$m_i\ddot{x}_i + 2k\sin^2\theta(2x_i - x_{i-1} - x_{i+1}) + c_d\dot{x}_i = F_{xi} \tag{4-10}$$

where:

$\ddot{x}_i$ = acceleration of particle P_i (m/s^2).

The global equations (for all layers) are obtained simply by applying equation(4-10) to each and every layer:

$$[M]\{\ddot{x}\} + [C_d]\{\dot{x}\} + [K]\{x\} = \{F_x\} \tag{4-11}$$

$$[M] = \begin{bmatrix} m_1 & 0 & \cdots & 0 & 0 \\ 0 & m_2 & 0 & \cdots & 0 \\ \cdots & \cdots & \cdots & \cdots & \cdots \\ 0 & 0 & \cdots & m_{n-1} & 0 \\ 0 & 0 & \cdots & 0 & m_n \end{bmatrix}_{n \times n} \tag{4-12}$$

$$[C_d] = \begin{bmatrix} c_{d1} & 0 & \cdots & \cdots & 0 \\ 0 & c_{d2} & 0 & \cdots & 0 \\ \cdots & \cdots & \cdots & \cdots & \cdots \\ 0 & \cdots & \cdots & c_{di} & 0 \\ 0 & 0 & \cdots & 0 & c_{dn} \end{bmatrix}_{n \times n} \tag{4-13}$$

$$[K] = 2k \sin^2 \theta \begin{bmatrix} 1 & -1 & 0 & 0 & 0 & 0 & \cdots & 0 \\ -1 & 2 & -1 & 0 & 0 & 0 & \cdots & 0 \\ 0 & -1 & 2 & -1 & 0 & 0 & \cdots & 0 \\ \cdots & \cdots & \cdots & \cdots & \cdots & \cdots & \cdots & \cdots \\ 0 & \cdots & 0 & -1 & 2 & -1 & 0 & 0 \\ 0 & \cdots & 0 & 0 & -1 & 2 & -1 & 0 \\ 0 & \cdots & 0 & 0 & 0 & -1 & 2 & -1 \\ 0 & \cdots & 0 & 0 & 0 & 0 & -1 & 2 \end{bmatrix}_{n \times n} \tag{4-14}$$

4.3 Numerical Solution

Because consolidation is assumed to be the result of wedge-in of the particles from one layer to the adjacent layers, there is no consolidation (compression) in the first layer representing the free surface of the material in the bin. This allows an assumption to be made that vibrational movement (not the total displacement) of the first layer is the same as the motion of the excitation: $X_1 \sin\omega t$. Therefore, the displacement vector in equation (4-11) has the form of:

$$\{x\} = \begin{Bmatrix} X_1 \sin 2\pi f t \\ x_2 \\ x_3 \\ \cdots \\ x_n \end{Bmatrix} = \begin{Bmatrix} X_1 \sin \omega t \\ x_2 \\ x_3 \\ \cdots \\ x_n \end{Bmatrix} \qquad (4\text{-}15)$$

where:

f = vibration frequency (Hz),

ω = angular frequency (1/s),

X_1 = amplitude of applied vibration (m), and

x_2 — x_n = displacement of layers 2 to n (m).

Furthermore, if no external dynamic forces are applied on the bulk solids during vibration, the force vector on the right-hand side of equation (4-11) is given as:

$$\{F_x\} = \{0\} \qquad (4\text{-}16)$$

A general solution of complex exponential functions to equation (4-11) is now given as (Beards, 1983; Davies, 1980):

$$\{x\} = \begin{Bmatrix} X_1 e^{pt} \\ X_2 e^{pt} \\ X_3 e^{pt} \\ \cdots \\ X_n e^{pt} \end{Bmatrix} = \begin{Bmatrix} X_1 \\ X_2 \\ X_3 \\ \cdots \\ X_n \end{Bmatrix} \cdot e^{pt} = \{X\} \cdot e^{pt} \qquad (4\text{-}17)$$

where:

$p = i\omega$,

i = unit of imaginary number, and

$X_1 - X_n$ = vibration amplitudes of layers 1 - n (complex numbers).

Substituting equations (4-16) and (4-17) into (4-11) yields:

$$\left\{p^2[M] + p[C_d] + [K]\right\}\{X\} = \{0\} \tag{4-18}$$

Equation 4-18 represents a set of *n* (number of layers) simultaneous equations and the first equation in the set is:

$$p^2 m_1 X_1 + p c_{d1} X_1 + 2k \sin^2\theta (X_1 - X_2) = 0 \tag{4-19}$$

The vibration amplitude for the second layer can be obtained from equation (4-19):

$$X_2 = \frac{p^2 m_1 + p c_{d1} + 2k \sin^2\theta}{2k \sin^2\theta} \cdot X_1 \tag{4-20}$$

Following the same procedure, equations for all layers can be solved consecutively for vibration amplitudes:

$$p^2 m_i X_i + p c_{di} X_i + 2k \sin^2\theta (-X_{i-1} + 2X_i - X_{i+1}) = 0 \tag{4-21}$$

$$X_{i+1} = \frac{(p^2 m_i + p c_{di} + 4k \sin^2\theta) X_i - 2k \sin^2\theta X_{i-1}}{2k \sin^2\theta} \tag{4-22}$$

for i = 2, 3, ……, n-1

When the vibration amplitude of each layer is calculated, compression (consolidation) between the two adjacent layers is determined as the difference in the amplitudes of the two layers and the total consolidation is calculated as the sum of compressions of each and every pair of adjacent layers.

4.4 Experiment

An experiment was conducted to validate the predictive model using a cylindrical container

(model bin) 150 mm in diameter and 292 mm in height. The bin was filled with red hard spring wheat which had an initial bulk density of 798 kg/m^3, kernel density 1439 kg/m^3, and internal friction angle φ of 25°. The wheat was poured continuously to the center of the bin from a small container located 50 mm above the bin. The vibration excitation was provided by a vibration table and an amplifier (400-Series-Vibrator and PA300 amplifier, Ling Dynamic Systems Limited, Royston, Hertfordshire, England). The vibrator was capable of generating vibration frequencies between 0 to 9000 Hz, and the maximum thrust force was 196 N. An accelerometer (Model 4366, B&K Ltd., Nærum, Denmark) was attached to the bottom of the model bin to measure vibration acceleration. Signals were fed to a conditioning amplifier (Model 2626, B&K Ltd., Nærum, Denmark) and analyzed by an oscilloscope (Model 2090-III, Nicolet Instrument Corporation, Madison, Wisconsin). The bin was subjected to vertical vibration at three frequencies (23Hz, 30Hz, and 48Hz). These are the frequencies that grain bins are likely to experience under normal operating conditions. Jones and Block (1996) studied the ground vibration caused by trains and found that the predominant frequency components was in the range of 4 to 30 Hz. Furthermore, machinery for bulk solids handling (electrical motors and internal combustion engines) usually cause vibrations at frequencies between 18 and 50 Hz (typically motors or engines running at speeds between 1000 to 3000 rpm). For each of the three frequencies, the vibration amplitude was gradually increased from the lowest level ($\approx$ 0) to the point where no further grain settlement occurred (the highest amplitude ever reached was 2.3 mm for 23 Hz tests). Little grain settlement was observed after the bin had been vibrated for 15 minutes at a given frequency and amplitude. Therefore, for each increment of amplitude, grain was allowed to settle for 15 minutes before a settlement reading was taken. Each test condition was replicated three times.

4.5 RESULTS AND DISCUSSION

Model parameters

Table 4-1 summarizes all the parameter values used in the model predictions. The structure angle θ is related to packing of particles in the bulk. This angle is 60° for both planer and spatial hexagonal packing of equal-sized spheres, which is the densest state of packed spheres of equal size. Consolidation is not possible if $\theta = 60°$. Based on the ratio of particle density to bulk density (1.804) the θ-angle of the tested wheat can be calculated.

If a cubic box with sides 10 times the diameter of particles is filled with particles, the number

of particles (N) that the box can hold is:

$$N = N_x N_y N_z \tag{4-23}$$

where N_x, N_y, and N_z are number of particles in the x, y and z directions, respectively, and they are calculated as follows for the densest packing condition ($\theta = 60°$)(fig. 4-3):

$$\left.\begin{aligned} N_x &= (2)(10)/(4\cos\theta) && = 10 \\ N_y &= (2)(10)/(1+2\cos\theta\sin 60°) && = 10.72 \\ N_z &= (2)(10)/\left[1+\sqrt{(\sin^2\theta - 0.5\tan^2 30°)}\right] && = 11.34 \end{aligned}\right\} \tag{4-24}$$

The ratio of particle density to bulk density at the densest packing condition is now calculated as:

$$R = \frac{(10d_p)(10d_p)(10d_p)}{N_x N_y N_z V_p} = \frac{(10d_p)(10d_p)(10d_p)}{(10)\ (10.78)\ (11.34)\left[\left(\frac{\pi}{6}\right)\left(d_p^3\right)\right]} = 1.562 \tag{4-25}$$

where:

R = particle density to bulk density ratio,

d_p = particle diameter (m), and

V_p = volume of a particle (m^3).

For the wheat tested, the ratio of particle density to bulk density was 1.804. Applying equations (4-24) and (4-25) yields:

$$\frac{(10d_p)(10d_p)(10d_p)}{[20/(4\cos\theta)]\,[20/(1+2\cos\theta\sin 60°)]\left[20/\left(1+\sqrt{\sin^2\theta - 0.5\tan^2 30°}\right)\right]\left[\left(\frac{\pi}{6}\right)\left(d_p^3\right)\right]} = 1.804 \tag{4-26}$$

Solving equation (4-26) for θ yields $\theta = 56.1°$ for the wheat tested (fig. 4-4).

The inter-layer rigidity k measures the deformability between two adjacent layers. Load-deformation tests were conducted to evaluate the inter-layer rigidity for wheat. In the tests, a cylindrical container with a diameter of 43 mm was used to contain a 10-mm grain column. For an equivalent kernel diameter of 5 mm. This 10-mm column of wheat represented approximately two (adjacent) vibration layers. A universal testing machine was used to applied 1.0 N force on the

sample through a 40-mm diameter compression ram. The average compressive deformation was 1.20 mm in 4 tests. Therefore, the inter-layer rigidity was calculated as 1.0 N/1.20 mm = 833.3 N/m. It should be noted that the inter-layer rigidity is dependent on the cross-sectional area of the grain column. Therefore, a unit area inter-layer rigidity k_A was determined as 6.63×10^5 N/m-m^2 (833.3 N/m $\div 1.26 \times 10^{-3}$ m^2, the area here is the cross-sectional area of the compression ram). The rigidity of the test bin, which had a diameter of 0.15 m, was calculated to be: $k = k_A \times (0.15\text{m}/2)^2 \times \pi = 11716$ N/m.

Model validation and predictions

The predicted total settlement of grain was in close agreement with the experimental data (figs. 4-5 to 4-7). To quantify the discrepancies between the model predictions and the data, overall average differences (OADs) were calculated by equation (4-27):

$$\text{OAD} = \frac{\sum |\text{measured} - \text{predicted}|}{\sum \text{measured}} \tag{4-27}$$

The calculated values of OAD were 17%, 8% and 11% for 23, 30 and 48 Hz tests, respectively. The highest discrepancy of 17% translates to a grain settlement of 3 mm. In other words, the predicted grain settlement was 3 mm off the measured value, which is about the size of a grain kernel.

Both measured data and predictions showed that grain settlement reached a maximum value at a certain amplitude and no further increase in settlement after this amplitude. Independent of vibration frequency, this maximum settlement was 30 mm, or 10.3% of the final initial grain depth. The bulk density corresponding to this maximum settlement was 890.6 kg/m^3. This appeared to be the highest density that could be achieved by vibrating the grain regardless of the frequency and amplitude. When the total grain mass and the bin diameter remains the same, the relative grain settlement (10.3% as calculated above) should be equal to the relative increase in bulk density numerically. The increase in bulk density was calculated as (890.6-797.6)/890.6 = 10.4%, which is almost identical to the relative gain settlement (10.3%). It is interesting to note that this maximum bulk density corresponds to a bulk-particle density ratio of 1.562, which is within 4% of the theoretical ratio of 1.618 for the hexagonally packed spheres of equal size.

The vibration frequency had a noticeable effect on the amplitude at which the maximum settlement was reached: the higher the frequency, the lower the amplitude for the maximum

settlement (fig. 4-5 to 4-7 and Table 4-2). This means that at higher frequency, less "shaking"(movement) is required to consolidate the grain.

The predicted variation of grain settlement with the bin height was not linear, with a higher settlement rate at the bin bottom than at the top (figs 4-8 and 4-9). For example, the increase in settlement with the grain depth through a 50-mm layer at the bin bottom was 23 times that through a 50-mm layer at the top when the vibration frequency was 30 Hz and amplitude 0.4 mm (fig. 4-8). Although neither the amplitude nor frequence had any effects on the maximum grain settlement, both had noticeable effects on the distribution of grain settlement in the grain mass before it reached the maximum, i.e., the higher the amplitude (or frequency), the quicker the settlement increased with the bin height. It is also interesting to note that the predicted curves of the grain settlement versus the grain depth (figs. 4-8 and 4-9) were not smooth. This wavy shape indicated that the consolidation of each grain layer in the bin was different depending on the vibration frequency and the properties of grain.

It should be mentioned that the maximum settlement (~10%) measured in this study may not occur in field conditions. Because a small bin was used in this study and it was possible to vibrate the bin thoroughly to achieve the densest packing condition in the bin. On the other hand, the vibration strength and duration for full-size bins would seldom result in the densest packing condition in the bins under field conditions. Therefore, the grain settlement in full-size bins should be less than that measured for the model in this study.

4.6 Conclusions

1. The vertical vibration of grain mass was adequately modeled by a one-dimensional spring-damper system. The model prediction of grain settlement (consolidation) was in good agreement with the experimental data for a model bin.
2. For the range of frequency (23 - 48 Hz) tested, the grain reached its maximum bulk density (theoretic limit) at different amplitudes. The higher the frequency, the lower the amplitude at which the maximum density (consolidation) occurred. The maximum density was independent of the vibration frequency.
3. The rate of consolidation within the grain mass increased with the grain depth in a nonlinear fashion. Both the amplitude and frequency affected the variation of grain consolidation with

the grain depth. A higher amplitude or frequency would result in a quicker increase of grain settlement with the bin height.

Table 4-1. Parameter values used in model predictions

Structure angle θ	56.1°
Unit area inter-layer rigidity k_A, N/m-m^2	6.63 x 10^5
Equivalent kernel diameter, mm	5.0
Kernel mass, kg	9.42 × 10^{-5}
Particle density ρ_p, kg/m^3	1439
Initial bulk density ρ (before vibration), kg/m^3	798
Internal friction angle φ	25°
Total depth of grain bulk Y_0, mm	292

Table 4-2. Vibration amplitudes at which the maximum settlement occurred

Frequency, Hz	Amplitude, mm		
	Measured	Predicted	Difference
23	0.78	0.93	19%
30	0.44	0.44	0%
48	0.39	0.18	-54%

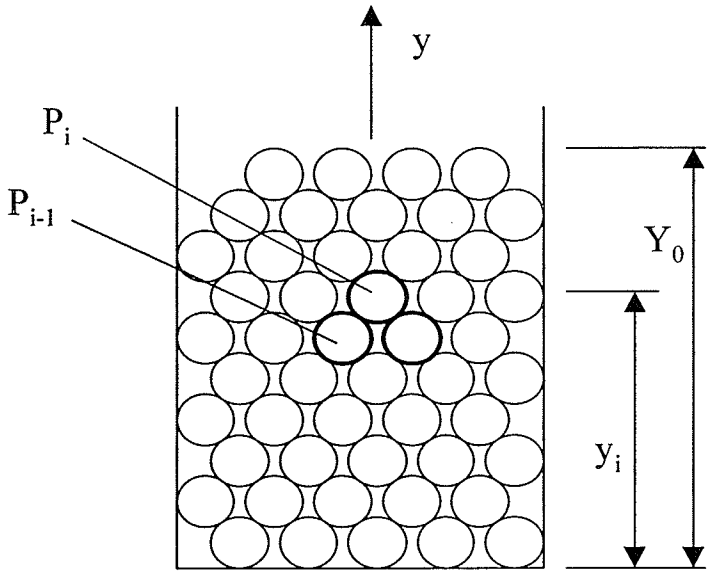

(a)

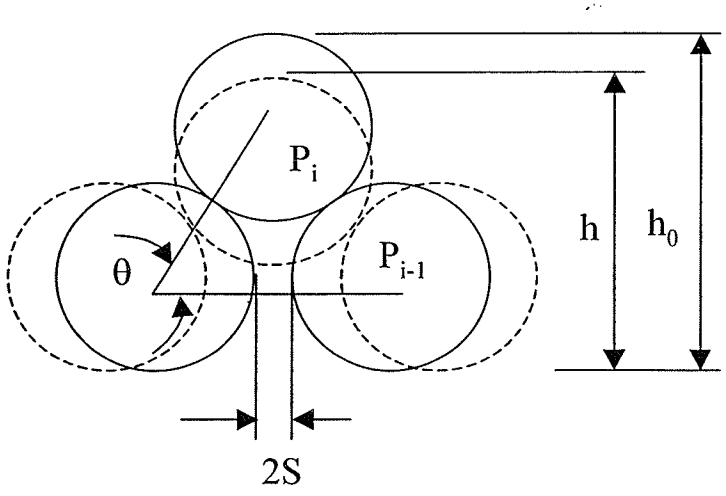

(b)

Figure 4-1. Schematics of particulate structure in storage bins, (a) layers of particles in a bin, (b) representative particles from the *i*th and (*i*-1)th layer

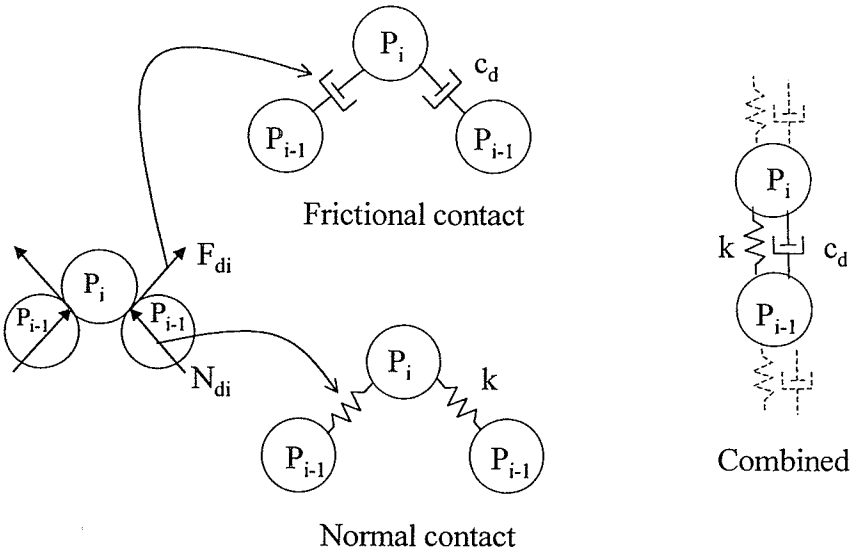

Figure 4-2. One-dimensional vibration model for bulk solids in storage bins

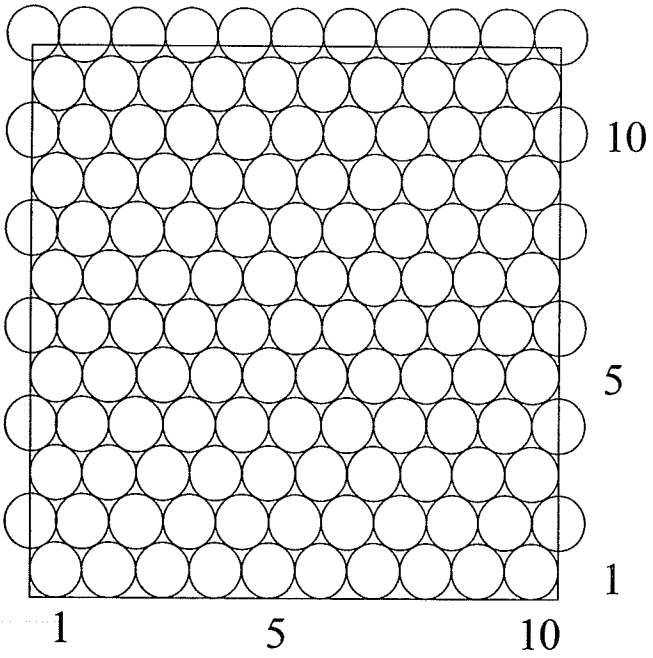

Figure 4-3. Hexagonal packing of equal-sized spheres (top view)

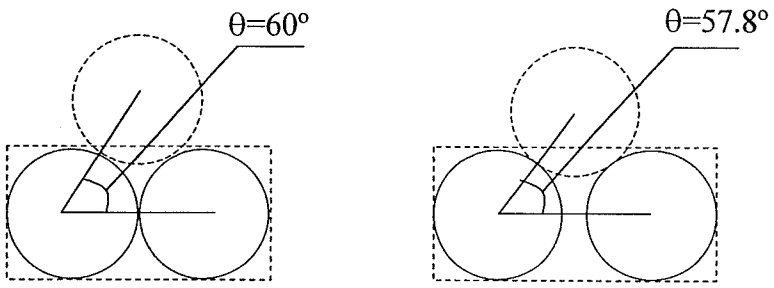

Figure 4-4. Schematic diagram for calculation of structure angle θ

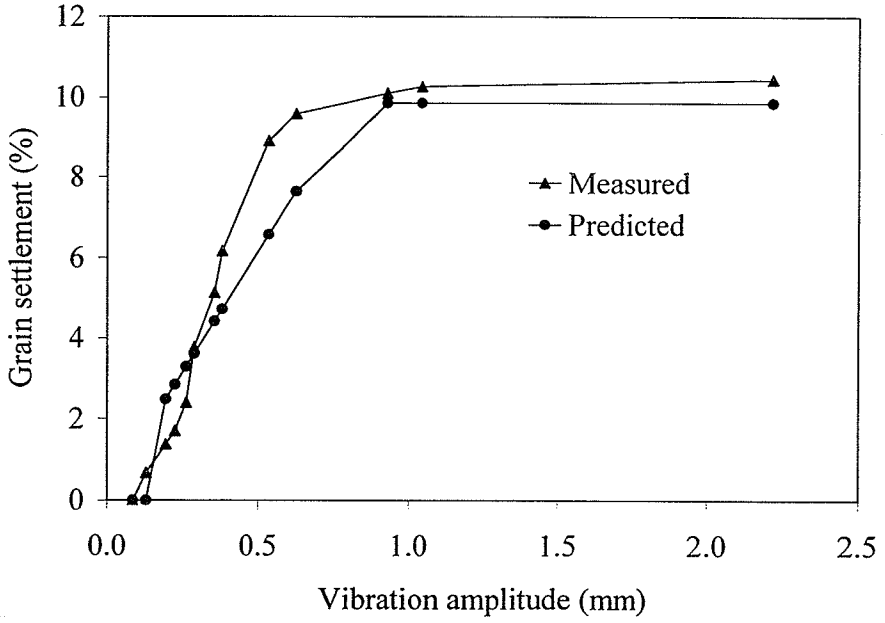

Figure 4-5. Comparison between measured and predicted total settlement of grain in model bin (23 Hz)

Figure 4-5. Comparison between measured and predicted total settlement of

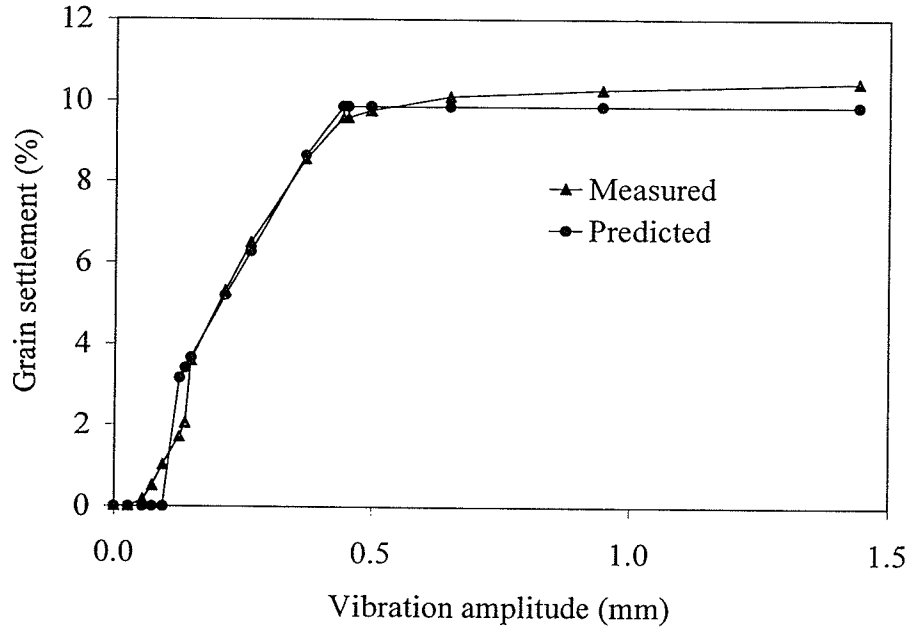

Figure 4-6. Comparison between measured and predicted total settlement of grain in model bin (30 Hz)

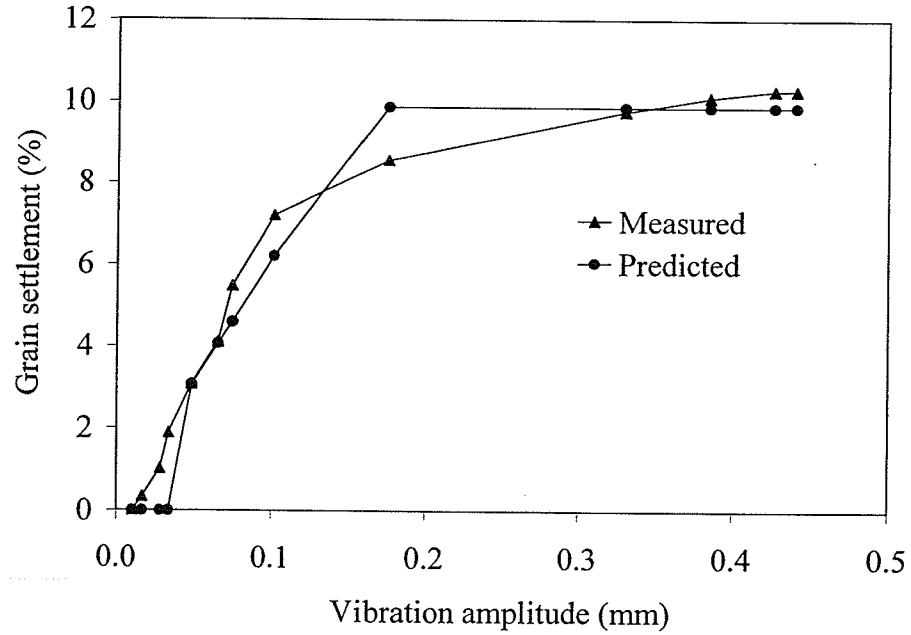

Figure 4-7. Comparison between measured and predicted total settlement of grain in model bin (48 Hz)

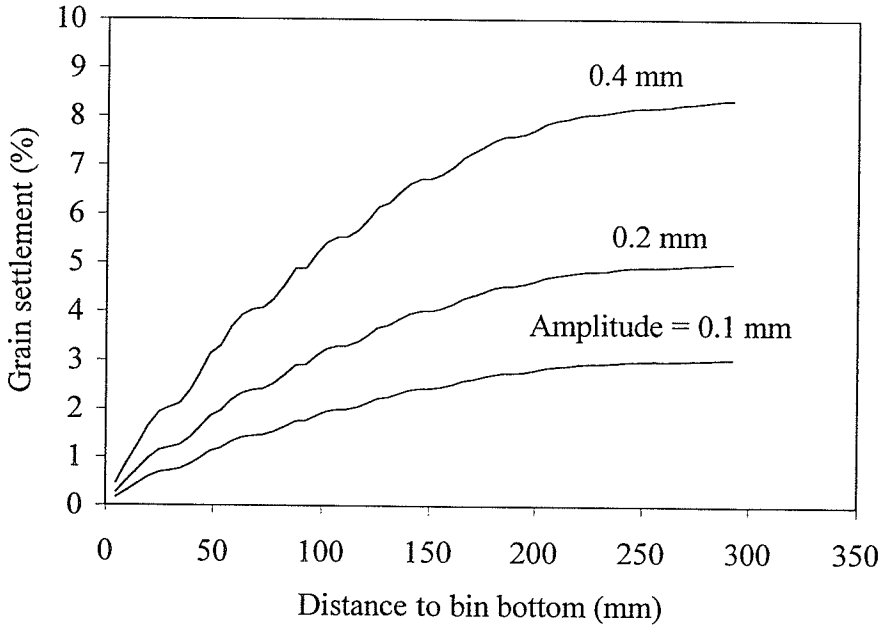

Figure 4-8. Predicted variation of settlement along grain depth (frequency = 30 Hz)

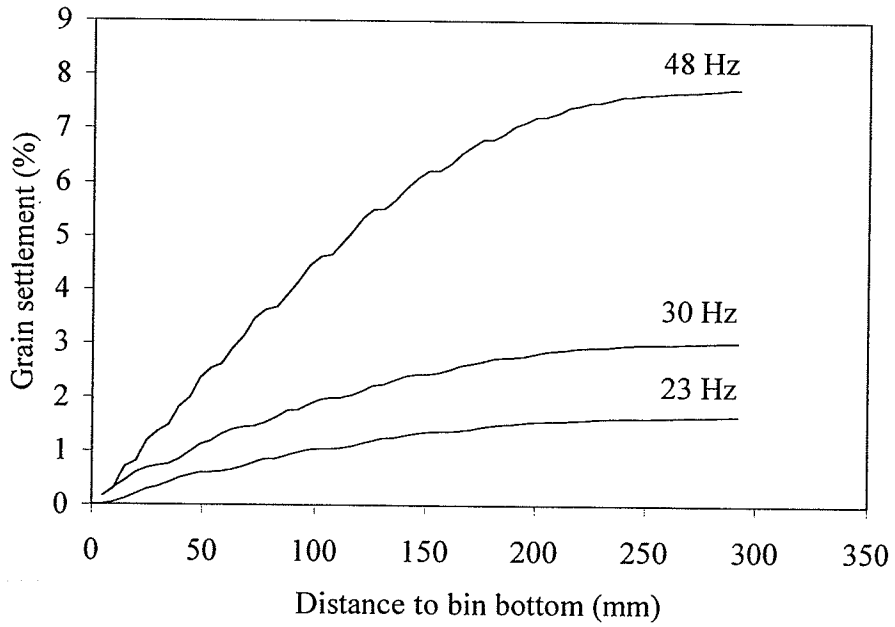

Figure 4-9. Predicted variation of settlement along grain depth (amplitude = 0.1 mm)

Chapter 5. LOADS IN GRAIN STORAGE BINS SUBJECT TO VERTICAL VIBRATION

Summary

A theory was proposed to calculate lateral pressures in bulk solids storage structures subject to vertical vibration. The theory assumes that the increases in lateral pressure in storage bins after vibration are caused by the changes in the direction of contact forces between particles and the lateral expansion of bulk solids induced by vibration. A close agreement with an average error of 8% was found between the predicted values of lateral pressure and the measured values reported in the literature.

5.1. Introduction

Vibration may change loads exerted by bulk solids on storage structures. A common explanation of increases in structure loads is that vibration causes increases in the density of bulk solids. However, Hao (1992) carried out an experiment in which a grain bin 1.0 m in diameter, 1.5 m in height was subjected to vertical vibration. He found that the grain bulk density increased 5% and the grain depth decreased 3% after 20 minutes of vibration. According to Janssen's equation (1895), a 5% increase in the bulk density would result in a 5% increase in lateral pressure at all depths, whereas a 3% decrease in grain depth would cause a 19% decrease in lateral pressure at the bin top and 3% at the bin bottom. Therefore, the net change in lateral pressure should be a decrease of 14% at the top level and an increase of 2% at the bottom level. This calculation did not agree with the measurements by Hao et al.(1994). They measured an increase of 39% in lateral pressure near the bin bottom (0.15 m from bin bottom). This means that there must be some other contributing factors besides the density and depth change. Hao et al. (1994) explained that lateral expansion was responsible for the large increase of lateral pressure after the bin was vibrated. However, they did not establish any theoretical model or feasible method to solve this problem. In the stipulations of a design code for bulk solid storage structures, it is important to estimate the loads on bulk solid storage structures when subjected to vertical vibration. The objective of this Chapter is to develop a model for predicting the pressure increase on the walls of bulk solid storage structures when subjected to vertical vibrations.

5.2. Model Development

Lateral pressure on the walls of a bin when subjected to vibration is assumed to be composed of three components: (1) static pressure, (2) pressure caused by the changes in the direction of contacts between particles, and (3) pressure due to the lateral expansion of bulk solids. The static pressure is calculated by Janssen's (1895) equation as follows:

$$p_{h0} = \frac{\rho R g}{\mu}\left[1 - e^{-\frac{K_a \mu y_i}{R}}\right] \qquad (5\text{-}1)$$

where:

p_{h0} = static lateral pressure (Pa),

ρ = grain bulk density (kg/m^3),

φ = internal friction angle (°),

μ = coefficient of friction of bulk solid on structure,

R = hydraulic radius (m),

K_a = lateral to vertical pressure ratio, $[(1-\sin\varphi)/(1+\sin\varphi)]$, and

y_i = depth (m).

A bulk solid material consists of solid particles and air spaces (voids). When external stresses are imposed on a bulk material, they are carried by the contact areas between particles. Vibration changes the fabric structure of the bulk material in a storage bin, and thus the distribution of contact forces changes. These changes re-distribute the gravity force (material weight) between the bin wall and the bin floor. If more material weight is shifted from the floor to the wall, an increase in lateral pressure occurs. To calculate this pressure increase caused by changes in particle contacts, a three-particle assembly is considered (fig.5-1). As mentioned in the previous Chapter, this assembly represents two vibration layers in the bin. The bottom two particles are denoted as the *i*th layer and the top one as layer (*i*+1). The initial contact angle (before vibration) between the *i*th particle and the contacting particle is θ which is the structure angle described in chapter 4, and the distance between the particle centroids in the two layers is h. There are three forces acting on the particles in contact with the wall (fig. 5-1). The resultant lateral force exerted on the particle by other particles (if it is amidst the bulk) or by the bin-wall (if it is in the boundary layer) is F_i; F_v is the resultant

vertical support force exerted on the particle (which includes bin-wall friction, friction from other particles, and the reaction from the lower layer); and F_u is the resultant force exerted by the contacting particle in the upper layer. Vibration causes the material to consolidate, and thus the distance between the two layers changes from h to h-Δh, and the contact angle changes from θ to θ-$\Delta\theta_i$ (fig. 5-1). Assume that the particle has no rotation, then all forces will pass through the center of the particle. A force diagram can be drawn to describe the forces on the *i*th particle after vibration assuming that the vertical force F_v remains unchanged (the total weight of the material above the *i*th layer remains the same) (fig. 5-2). Because the bin-wall was assumed to be perfectly rigid and the neighboring particles have the same relative position change, the distance AB between the centers of two particles will stay the same after vibration (compression of particles will be discussed in the following section). From the geometric relationships shown in figure 5-2, following equations are obtained:

$$\frac{h}{AB} = \frac{F_v}{F_h} \quad \text{and} \quad \frac{h-\Delta h}{AB} = \frac{F_v}{F_h'} \tag{5-2}$$

Combining the above two equations yields:

$$\frac{F_h'}{F_h} = \frac{h}{h-\Delta h} \tag{5-3}$$

or:

$$F_h' = \frac{hF_h}{h-\Delta h} \tag{5-4}$$

where:

F_h = lateral force exerted on a particle before vibration (N),

F'_h = lateral force exerted on a particle after vibration (N),

F_v = vertical force exerted on a particle (N),

AB = half the distance between the centers of two neighboring kernels at a same layer (mm),

h = layer thickness (mm),

Δh = consolidation for each layer (mm),

The force predicted by equation (5-4) is divided by the contact area between the bin-wall and the material layer obtain the lateral pressure:

$$p'_h = \frac{hp_{h0}}{h - \Delta h} \tag{5-5}$$

where:

p'_h = lateral pressure after vibration, (Pa).

The lateral pressure calculated by equation (5-5) includes the static lateral pressure and an additional pressure induced from the change in particle contacts. The net increase in lateral pressure can be expressed as:

where:

$$p_{hI} = p'_h - p_{h0} = \frac{\Delta hp_{ho}}{h - \Delta h} \tag{5-6}$$

p_{hI} = increase in lateral pressure induced by the change in particle contacts (Pa).

In Chapter 4, a wedge-in theory was proposed to predict the fabric changes in bulk solids subject to vertical vibrations. The theory hypothesizes that vibration causes the bulk solids to consolidate vertically, as well as to expand laterally. However, the lateral expansion of bulk solids in a bin will be resisted by the bin walls, thus additional pressure is induced on the bin walls. This induced pressure is associated with the elastic force of compressed particles. To calculate the pressure increase associated with the lateral expansion, the expansion process is assumed to occur in two steps: 1) the bulk material expands freely, and 2) the bin walls compress the bulk solid back to its actual size. The pressure required to compress the bulk solid is the pressure increase induced by the lateral expansion. As it is shown in figure 5-3a, when the center of an upper particle moves from O to O' by vibration, the center distance between the two particles changes from AO to AO'. If assuming the bin wall is perfectly rigid, the compression (along the center line of particle A and O) that the *i*th particle A is experiencing is approximately equal to the length of OB ($\Delta\theta$ is very small). Mathematically:

$$d \approx OB = \Delta h \cdot \sin\theta \tag{5-7}$$

where:

d = particle compression (m), and

θ = structure angle.

For each layer, the area through which the compression force is transferred to the wall is:

$$S_1 = \pi \times D \times h \tag{5-8}$$

where:

S_1 = loading area (m^2),

D = diameter of the bin (m), and

h = layer thickness (m).

Thus for a whole layer which is consolidated for the amount of Δh, the lateral pressure caused by compression is:

$$p_{h2} = k_A \cdot S \cdot OB \cdot \cos\theta / S_1 = k_A S \Delta h \sin\theta \cos\theta / S_1 \tag{5-9}$$

where:

p_{h2} = lateral pressure induced by compression (Pa),

k_A = unit area rigidity (N/m-m^2), and

S = cross section area of the bin (m^2).

The total lateral pressure on the bin wall after vibration is now determined as the sum of the three components:

$$p_h = p_{ho} + p_{h1} + p_{h2} \tag{5-10}$$

A C++ code was developed to calculate the total lateral pressure for bulk solids storage bins subjected to vertical vibration (Appendix B). To use equations (5-6) and (5-9) the consolidation Δh

is numerically calculated using the method described in Chapter 4.

5.3. Results And Discussion

Model predictions are compared with the experimental data reported by Hao et al. (1992) for a model bin filled with wheat. The bin was 1.0 m in diameter and 1.5 m high, and subjected to 20 minutes of vibration at a frequency of 30 Hz. The total consolidation was measured as 50 mm by Hao et al. (1992). Other parameters used in the model prediction are described in Chapter 4 and summarized in Table 5-1. The grain bulk was divided into 300 layers, with each layer having a thickness of 5 mm (assumed diameter of grain kernel). The lateral pressure predicted by the model in each layer represents the pressure exerted by a single kernel on the bin wall. However, the average pressure is often of interest. The predicted lateral pressures are therefore averaged over 10 adjacent layers.

Predicted lateral pressures are in close agreement with the data of Hao et al. (1992) for wheat at moisture contents of 12% (fig. 5- 4). The measured lateral pressure averaged over 6 points along the depth of the model bin is 2541.7 Pa. The corresponding predicted average lateral pressure is calculated as 2736.9 Pa. The average error is 8%. In contrast, the Janssen's predictions are lower than the measured values with an average value of 1924.3 Pa. The difference is 24.29%.

The predicted lateral pressure follows a wavy curve along the grain depth. This is attributed the existence of multiple vibration modes. The curve shape depends on the vibration frequency and other characteristics of vibration. This distribution pattern indicates that the increase in lateral pressure is not uniform in the bin after vibration. In some locations, the pressure remains almost at the same level as the static pressure, whereas the pressure is 2.2 times higher than the static pressure near the bin bottom.

For a full size bin with 4 m in diameter and 6 m in height the comparison between the predicted lateral pressure by the numerical model and by Janssen's calculation is shown in fig. 5-5. At the bin bottom, if the same vibration amplitude and frequency as described in Hao's experiment (Hao et al., 1992) were exerted, the lateral pressure predicted by the numerical model is about 50% larger than Janssen's value. When the vibration frequency changes from 30 Hz to 60 Hz and the input vibration energy remains the same, the predicted lateral pressure increases slightly. When the vibration frequency remains to be 30 Hz, but the consolidation becomes 1/10 of the original

consolidation, the predicted lateral pressure at the bin bottom becomes about 5% larger than Janssen's value.

5.4. Conclusions

1. The model adequately predicts the lateral pressure on the bin wall after vibration. The difference between the predicted pressure and those measured by Hao et al. (1992) are between 0.025 to 0.35 kPa, or 1% to 12%.
2. The predicted vibration-induced pressure increase is not uniform in the bin. The greatest increase in lateral pressure after vibration is 2.2 times the static pressure near the bin bottom for a 1.5 m height model bin.
3. For a full size bin with 4 m in diameter and 6 m in height the predicted vibration-induced pressure had a similar wavy shape as for a 1.5 m height model bin. The lateral pressure predicted by the numerical model is about 50% larger than Janssen's value.
4. Vibration energy has the most significant influence on the predicted lateral pressure. The more vibration energy, the more increase in lateral pressure. Vibration frequency has slight effect on lateral pressure. Higher frequency will increase the predicted lateral pressure slightly.

Table 5-1. Parameter values used in lateral pressure predictions

θ-angle	56.1°
unit area inter-layer rigidity, N/m	6.63e5
Bulk density, kg/m^3	798
Internal friction angle	25°
Wall friction coefficient	0.43

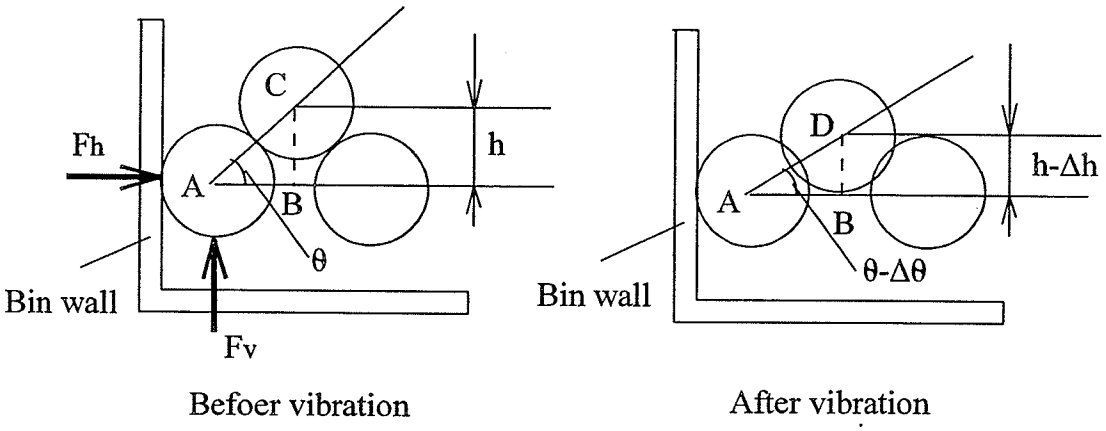

Figure 5-1. Relative position of kernels before and after vibration

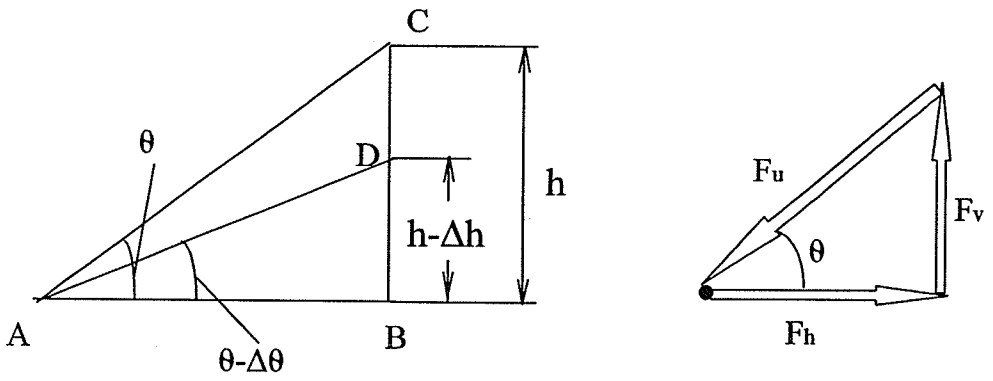

Figure 5-2. Element orient triangles and force triangles

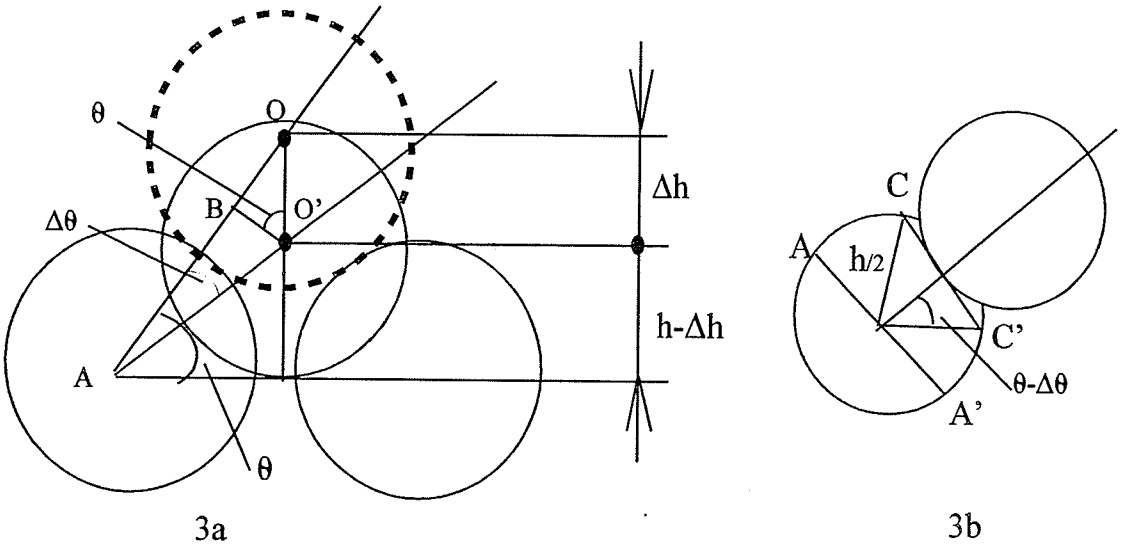

Figure 5-3. - Schematic diagram of kernel compression

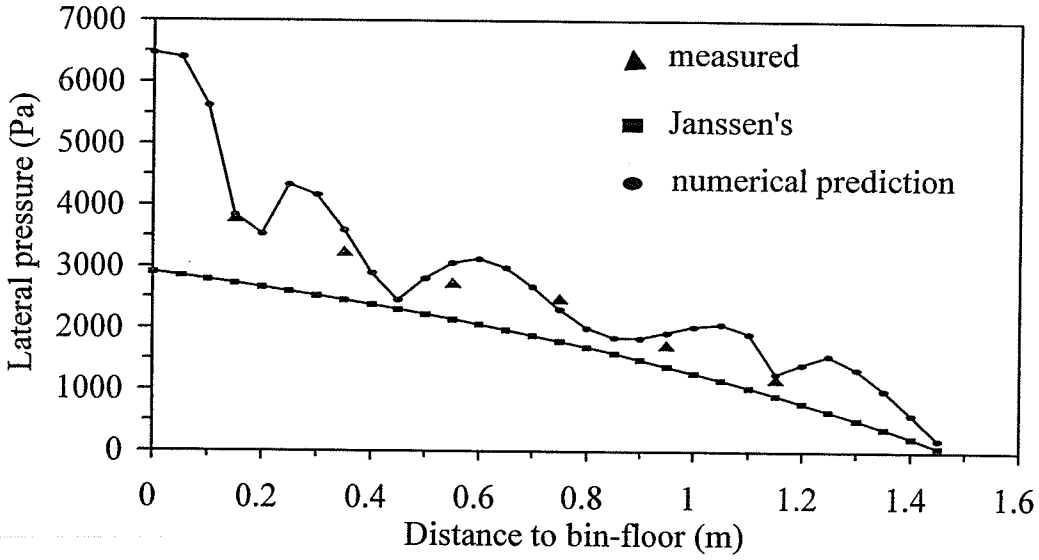

Figure 5-4. Comparison between calculated and measured lateral pressure

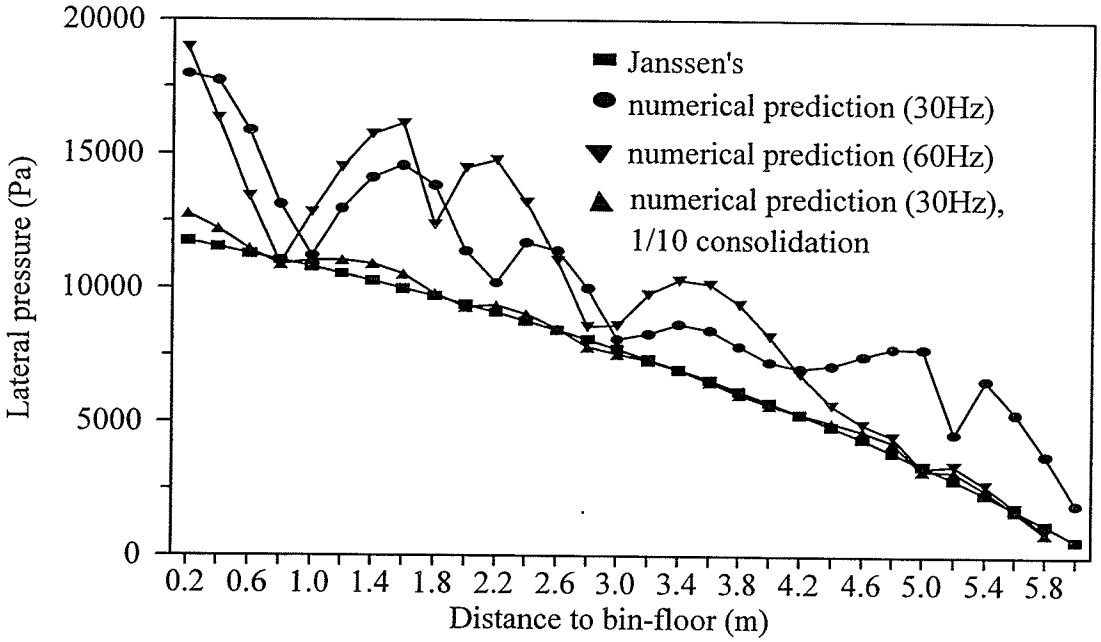

Figure 5-5. Comparison of lateral pressure between numerical prediction and Janssen's calculation

Chapter 6. NUMERICAL SOLUTION FOR EIGENVALUES AND EIGENVECTORS OF BULK SOLIDS STORAGE SYSTEM

Summary

Eigenvalues and eigenvectors are among the most important parameters for characterizing the behavior of bulk solid storage structures when subjected to vibration. Because of the large number of degrees of freedom, there exist no analytical solutions to eigenvalues and eigenvectors for bulk solid systems subject to vibration. In this chapter, an inverse superposition method was developed to numerically determine the eigenvalues and eigenvectors for grain storage systems. The predicted results were in good agreement with experiential data obtained from model bin tests. The first three natural frequencies were predicted to be 2.0, 6.1, and 10.2Hz, respectively, for a 292 mm high grain column, while the corresponding measured values were 3.5, 7.0, and 11.0 Hz.

6.1. Introduction

Bulk solids consist of solid particles and voids and their properties change with the operating conditions in the handling facilities. Vibration causes changes in the spacial arrangement of particles in bulk solids. The characteristics of vibration in bulk solid systems are dependent on the type of bulk solid storage structures. The vibration characteristics are quantified by the natural frequencies (eigenvalues) and vibration mode (eigen vectors). In the industry, the idea of using vibratory devices to prevent arch formation has been attempted but with limited success. One possible important reason is the lack on the understanding of the vibrational characteristics of the bulk solid systems. Different vibration frequency and mode will exert a different effect on the dynamic behavior of the bulk material. Only suitably selected vibration frequencies and modes are effective in delivering energy for arch destruction. Thus, in applying vibration to bulk solid systems for arch destruction, it is important to develop appropriate methods for selecting the most effective vibration frequencies and modes. For this reason, a numerical model was developed focusing on predicting the eigenvalues and eigenvectors.

6.2. Mechanics Mathematic Models

To determine the eigenvalues and eigen vector for a bulk solid system, a mechanics model has to be established. It is shown in Chapter 4 that the vertical vibration of a bulk solid system can

be represented by a spring-damper system (fig. 6-1). The equation to calculate the eigenvalue and eigenvector of the system now become (Hatter, 1973):

$$[K]\{X\} = \omega^2[M]\{X\} \tag{6-1}$$

where:

ω = natural angular frequencies of the system (rad/s), and

$\{X\}$ = amplitude vector of the system (m).

The coefficient matrixes for the system were derived as follows:

$$[M] = \begin{bmatrix} m_1 & 0 & \cdots & 0 & 0 \\ 0 & m_2 & 0 & \cdots & 0 \\ \cdots & \cdots & \cdots & \cdots & \cdots \\ 0 & 0 & \cdots & m_{n-1} & 0 \\ 0 & 0 & \cdots & 0 & m_n \end{bmatrix} \tag{6-2}$$

$$[K] = 2k_e \sin^2\theta \begin{bmatrix} 1 & -1 & 0 & 0 & 0 & 0 & \cdots & 0 \\ -1 & 2 & -1 & 0 & 0 & 0 & \cdots & 0 \\ 0 & -1 & 2 & -1 & 0 & 0 & \cdots & 0 \\ \cdots & \cdots & \cdots & \cdots & \cdots & \cdots & \cdots & \cdots \\ 0 & \cdots & 0 & -1 & 2 & -1 & 0 & 0 \\ 0 & \cdots & 0 & 0 & -1 & 2 & -1 & 0 \\ 0 & \cdots & 0 & 0 & 0 & -1 & 2 & -1 \\ 0 & \cdots & 0 & 0 & 0 & 0 & -1 & 2 \end{bmatrix}_{n \times n} \tag{6-3}$$

where:

[M] = mass matrix (kg),

[K] = stiffness matrix (N/m),

m_i = mass of the ith layer (kg),

k_e = inter-layer stiffness (stiffness between the two adjacent layers) (N/m), and

θ = structure angle (°).

6.3. Solution Procedure

To calculate the eigenvalues and eigenvectors for the system described by equation (6-1), let the n eigenvalues and eigenvectors of the system be ω_1^2, ω_2^2, $\cdots$ ω_n^2 and ϕ_1, ϕ_2, $\cdots$,ϕ_n, respectively. Assuming that there is no rigid body motion, i.e. $\omega_1 \neq 0$, then, all the n eigenvalues and eigenvectors should satisfy equation (6-1). Thus following equation can be obtained:

$$[K][\Phi][\Omega] = [M][\Phi] \tag{6-4}$$

where:

$$[\Phi] = \left[\phi_1, \quad \phi_2, \quad \cdots, \quad \phi_n\right],$$

$$[\Omega] = \text{diagonal}\left[\frac{1}{\omega_1^2}, \quad \frac{1}{\omega_2^2}, \quad \cdots, \quad \frac{1}{\omega_n^2}\right] \quad .$$

By multiplying an arbitrary vector $\{a_0\} = \{a_{01}, \quad a_{02}, \quad \cdots, \quad a_{0n}\}^T$ on both sides of equation (6-4) yields:

$$[K][\Phi]\{a_1\} = [M][\Phi]\{a_0\} \tag{6-5}$$

where:

$$\{a_1\} = [\Omega]\{a_0\} = \frac{1}{\omega_1^2}\left[a_{01}, \quad \frac{\omega_1^2}{\omega_2^2}a_{02}, \quad \cdots, \quad \frac{\omega_1^2}{\omega_{n2}^2}a_{0n}\right]^T \tag{6-6}$$

Repeating the procedure s times yields:

$$\{a_s\} = [\Omega]\{a_{s-1}\} = [\Omega]^s\{a_0\} = \frac{1}{(\omega_1^2)^s}\left[a_{01}, \quad \left(\frac{\omega_1^2}{\omega_2^2}\right)^s a_{02}, \quad \cdots, \quad \left(\frac{\omega_1^2}{\omega_n^2}\right)^s a_{0n}\right]^T \tag{6-7}$$

The first subscript of the elements in vector $\{a\}$ denotes the number of superposing and the second subscript denotes the position of the element in vector $\{a\}$. Because the first natural frequency is

lower than all the other natural frequencies, if the superposing number s is large enough, item $\left(\frac{\omega_1^2}{\omega_i^2}\right)^s$ will tend to an infinitesimal. Thus, vector $\{a_s\}$ will gradually become parallel to vector $\{a_{01},\ 0,\ \cdots,\ 0\}^T$, i.e.,

$$\{a_s\} \approx \left(\frac{1}{\omega_1^2}\right)^s \{a_{01},\ 0,\ \cdots,\ 0\}^T \tag{6-8}$$

The ratio of modules between any two successive superposing vectors will converge to the square of first eigenvalue (Hatter, 1973):

$$\frac{1}{(\omega_1^2)^2} = \frac{\{a_s\}^T\{a_s\}}{\{a_{s-1}\}^T\{a_{s-1}\}} \tag{6-9}$$

If $\{X_0\} = [\Phi]\{a_0\}$ is used as the initial vector before superposing, and $\{X_1\} = [\Phi][\Omega]\{a_0\}$ the vector after the first superposing, then the first eigenvalue and eigen vector can be obtained from iterations of superposition. To calculate the next higher eigenvalue and eigenvector, we only need to create a new arbitrary initial vector in superposition which is orthogonal to all known eigenvectors, and then repeat the same superposing procedure. The algorithm of calculating the eigenvalues and eigenvectors using the inverse superposing method is summarized as follows.

(1) Assign arbitrary values to the amplitude vector {X}, say:

$$\{X^{(1)}\} = \{1,\ 0,\ 0,\ \cdots\cdots,\ 0,\ 0\}^T_{n\times 1} \tag{6-10}$$

(2) Calculate a derived vector from the initial values of the amplitude vector:

$$\{Y^{(1)}\} = [M]\{X^{(1)}\} \tag{6-11}$$

(3) Calculate an improved amplitude vector $\{X^{(2)}\}$:

$$[K]\{X^{(2)}\} = \{Y^{(1)}\} \tag{6-12}$$

(4) Repeat the process:

$$[K]\{X^{(k+1)}\} = \{Y^{(k)}\} \tag{6-13}$$

$$\{Y^{(k+1)}\} = [M]\{X^{(k+1)}\} \tag{6-14}$$

(5) At each iteration, calculate an approximate eigenvalue (6-15) until it meets the precision criterion (6-16):

$$\lambda^{(k+1)} = \frac{\{X^{(k+1)}\}^T\{Y^{(k)}\}}{\{X^{(k+1)}\}^T\{Y^{(k+1)}\}} \tag{6-15}$$

$$\frac{\lambda^{(k+1)} - \lambda^{(k)}}{\lambda^{(k+1)}} \leq \varepsilon \tag{6-16}$$

where:

λ = eigenvalue ($1/s^2$),

$\varepsilon = 10^{-8}$.

(6) If equation (6-16) is not satisfied, then calculate an improved initial vector and go to Step 4 for the next iteration:

$$\{Y^{(k+1)}\} = \frac{\{Y^{(k+1)}\}}{\left(\{X^{(k+1)}\}^T\{Y^{(k+1)}\}\right)^{\frac{1}{2}}} \tag{6-17}$$

(7) Otherwise, calculate the first natural frequency, the first natural mode:

$$f_1 = \frac{\omega_1}{2\pi} = \frac{\sqrt{\lambda^{(k+1)}}}{2\pi} \tag{6-18}$$

$$\{\phi\}_1 = \frac{\{X^{(k+1)}\}}{(\{X^{(k+1)}\}^T\{Y^{(k+1)}\})^{\frac{1}{2}}} \tag{6-19}$$

(8) After the lower j-1 eigenvectors are obtained, the jth eigenvalue and eigenvectors are obtained by constructing a new initial vector by making it orthogonal to j-1 eigenvectors:

$$\{X\}_j^{(1)} = \{X\}_j^a - \sum_{i=1}^{j-1} \beta_i \{\phi\}_i \qquad (i = 1, 2, \cdots\cdots, j-1) \tag{6-20}$$

where

$\{X\}_j^a$ = an arbitrarily built vector

$$\beta_i = \{\phi\}_i^T [M]\{X\}_i^a \qquad (i = 1, 2, \cdots\cdots, j-1) \tag{6-21}$$

Then repeat above iteration procedure from step1 to step 7. A C++ program was developed to conduct above algorithm (Appendix C).

6.4. Verification of the Numerical Model with a Theoretical Example

To verify the accuracy of the numerical model, model predictions were compared with the analytical solutions for a simple system with 3-degrees of freedom (fig.6-2). The motion equation for this system is (Steidel, 1979):

$$\begin{bmatrix} m & 0 & 0 \\ 0 & m & 0 \\ 0 & 0 & m \end{bmatrix} \begin{Bmatrix} \ddot{x}_1 \\ \ddot{x}_2 \\ \ddot{x}_3 \end{Bmatrix} + k \begin{bmatrix} 1 & -1 & 0 \\ -1 & 2 & -1 \\ 0 & -1 & 2 \end{bmatrix} \begin{Bmatrix} x_1 \\ x_2 \\ x_3 \end{Bmatrix} = \begin{Bmatrix} 0 \\ 0 \\ 0 \end{Bmatrix} \tag{6-22}$$

where:

m = mass of the object (kg),

k = rigidity of the spring (N/m),

$\ddot{x}_i$ = acceleration of a mass (m/s^2), and

x_i = displacement of a mass (m).

The theoretical values of three natural frequencies are (Steidel, 1979):

$$\begin{Bmatrix} f_1 = \dfrac{\sqrt{0.198k/m}}{2\times\pi} \\ f_2 = \dfrac{\sqrt{1.55k/m}}{2\times\pi} \\ f_3 = \dfrac{\sqrt{3.25k/m}}{2\times\pi} \end{Bmatrix} \quad \text{Hz} \tag{6-23}$$

For k =100000 N/m and m=100 kg, the theoretical values of natural frequencies are calculated as follows:

$$\begin{Bmatrix} f_1 = \dfrac{\sqrt{0.198\times 100000/100}}{2\times 3.14159} = 2.2395 \ \text{(Hz)} \\ f_2 = \dfrac{\sqrt{1.55\times 100000/100}}{2\times 3.14159} = 6.266 \ \text{(Hz)} \\ f_3 = \dfrac{\sqrt{3.25\times 100000/100}}{2\times 3.14159} = 9.0732 \ \text{(Hz)} \end{Bmatrix} \tag{6-25}$$

The three theoretical eigenvectors are:

$$\begin{Bmatrix} \{\phi\}_1 = \{2.247 \quad 1.802 \quad 1.000\}^T \\ \{\phi\}_2 = \{-0.802 \quad 0.445 \quad 1.000\}^T \\ \{\phi\}_3 = \{0.555 \quad -1.247 \quad 1.000\}^T \end{Bmatrix} \tag{6-24}$$

The corresponding values of natural frequencies predicted by the numerical models are: 2.2400, 6.2783 and 9.0611 Hz, respectively. The numerical predications and analytical solutions were almost identical. The comparisons of eigenvectors between the numerical model and the analytical solutions are summarized in Table 6-1. Again, the two methods resulted in almost the same eigenvalues.

6.5. Verification of the Numerical Model with the Experimental Data

Further validation was conducted by comparing the numerical predictions with experimental data. Vibration tests were carried out using a model grain bin 150 mm in diameter and 292 mm in

height. The bin was filled with wheat which had a layer rigidity k_e=6.63x10^5 N/m (Chapter 4). In the numerical simulations, the grain mass in the bin was divided into 60 layers. The measured particle density and bulk density were 1438.8 and 797.57 kg/m^3, respectively. Based on the ratio of particle density to bulk density (1.804), the θ-angle was calculated to be 57.8°. With the numerical model, the first three natural frequencies were calculated as 2.044, 6.131, and 10.210 Hz, respectively.

To measure the corresponding natural frequencies of the grain bulk system, an accelerometer was placed on the top free surface of the grain mass to measure the vibration of the top grain layer. The schematic diagram for the measurement is shown in fig.6-3. Because the top layer of the grain mass is a free end of the vibration system, it will always be a peak position of the system for any resonant vibration mode (Timoshenko et al., 1974). That is, for any natural frequency the grain mass system vibrates at, the top layer will be a peak in the corresponding vibration shape. Thus, for any input vibration amplitude, the output vibration amplitude at top layer of the grain mass system will reach a local maximum value for any of the natural frequencies. In other words if the ratio of the output amplitude at top layer to the inputted vibration amplitude reaches a local maximum value at a certain frequency, this frequency is a natural frequency of the grain mass system. Because of the limitation of the experimental equipment, the vibrator minimum frequency is 3 Hz. The frequency was first roughly scanned from 3 Hz to 15Hz and three peaks approximately within the ranges of 3-4 Hz, 6-8 Hz, and 10-12 Hz respectively were observed. Then within each range, three frequencies at a constant step increase were selected to measure the vibration amplitudes from both the top layer and the base of the model bin. The measured values are listed in Table 6-2. The ratios of output amplitude at top layer of grain mass to the inputted vibration amplitude are also listed in Table 6-2 and are plotted in fig. 6-4.

From Table 6-2 and fig. 6-4, the measured natural frequencies were found to be 3.5, 7.0, and 11 Hz, which compare favorably with the calculated values of 2.044, 6.131, and 10.210 Hz.

6.6. Conclusion

The numerical model developed in this study was adequate in predicting natural frequencies and eigenvectors of a grain storage system. The average difference in the lowest 3 natural frequencies between the numerical solution and measured values was about 1 Hz for a model grain bin filled with wheat.

Table 6-1. Comparison of eigenvectors between numerical prediction and analytical solution

	Analytical	Numerical
1st eigenvector	$\{2.247, 1.802, 1.000\}^T$	$\{2.258, 1.806, 1.000\}^T$
2nd eigenvector	$\{-0.802, 0.445, 1.000\}^T$	$\{-0.813, 0.490, 1.000\}^T$
3rd eigenvector	$\{0.555, -1.247, 1.000\}^T$	$\{0.459, -1.147, 1.000\}^T$

Table 6-2. Measured vibration amplitudes and their ratios

Frequency (Hz)	Base vibration (input) amplitude (mm)	Top vibration amplitude (mm)	Ratio (Top/Base)
3	3.71	4.05	1.09
3.5	1.82	3.0	1.65
4	1.03	0.77	0.75
6	0.37	0.73	1.97
7	0.43	1.02	2.37
8	0.47	0.85	1.81
10	0;.70	0.61	0.87
11	0.40	0.63	1.58
12	0.37	0.54	1.46

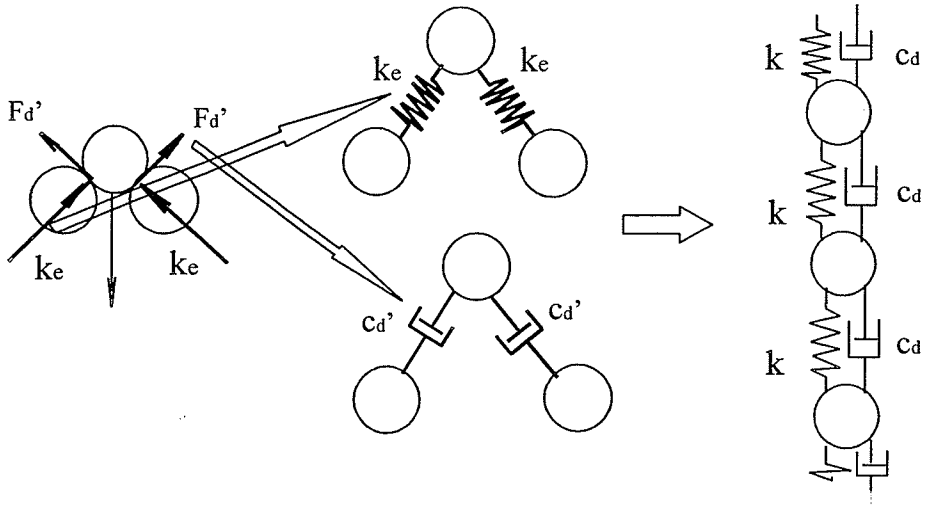

Figure. 6-1. Diagram of vibration model for a grain mass system

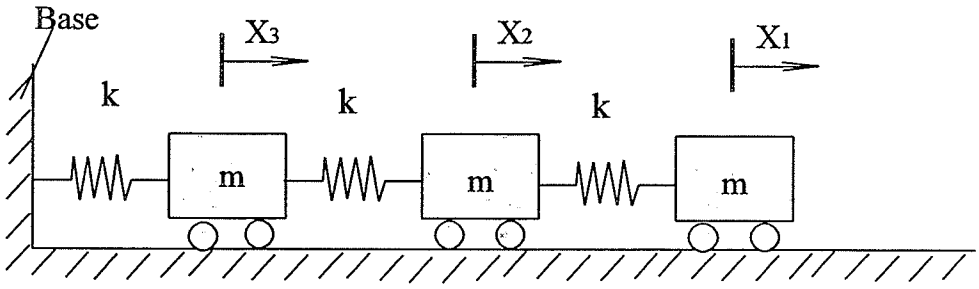

Figure. 6-2. Schematic diagram of a vibration system with 3 degrees of freedom

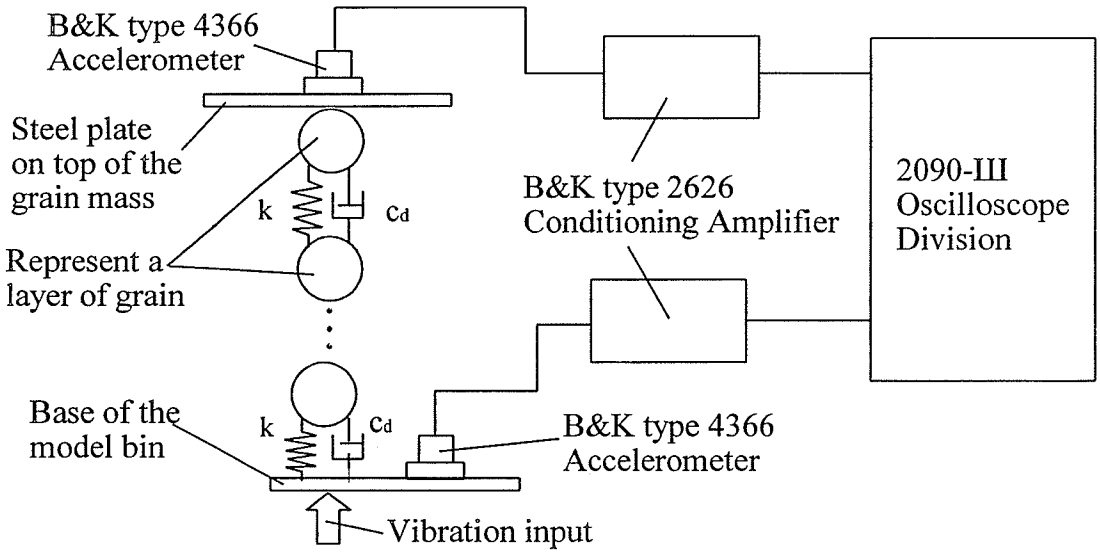

Figure 6-3. Schematic diagram for the measurement of natural frequencies

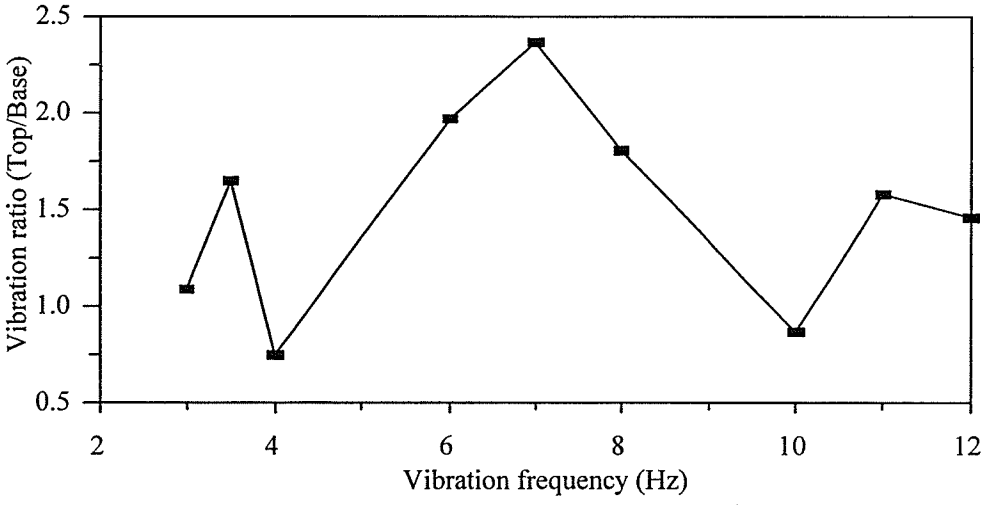

Figure 6-4. Ratios of output vibration amplitude at top layer to the inputted amplitude

Chapter 7. THEORETICAL ANALYSIS OF ARCH DESTRUCTION IN STORAGE BINS DURING VIBRATION

Summary

Theoretical criteria have been developed for arch destruction by vertical vibration in storage bins for cohesive bulk solids. The theory considers the force equilibrium on an arch and the cohesive material system is simulated as thin layers connected by elastic and damping elements during vibration. The theory predicts the minimum acceleration amplitudes and thrust forces required for destroying arches at certain locations in storage bins. It is theoretically proven that the optimal vibration frequency for arch destruction is one of the natural frequencies of the cohesive material system.

1. Introduction

Improving flow of cohesive bulk solids in storage bins has been a challenge to researchers and designers. Various flow enhancing devices, such as air blasters, vibrators, chain slingers, and bin inserts have been studied and used to improve flow in storage bins (Johanson, 1967; Grossman et al., 1990). Myers (1970), Suzuki and Tanaka (1972), Carroll and Colin (1975), and Roberts et al. (1979; 1986) explored the effect of vibration on bulk solids flow, and studied vibration as a possible solution to the flow problems of bulk solids. Wes et al. (1990) proposed a method for controlling flow of cohesive powders by simultaneous aeration and vibration. An experiment conducted by Tardos and Lu (1996) showed that the presence of a vibrator on the discharge hopper had a significant role in improving both the overall material flow and the feeding precision of a screw feeder. As a means of flow promotion, vibration energy should be transmitted through the material in a way which will ensure a reduction in shear strength in the critical regions of the flow obstruction (Roberts et al., 1979). Arnold and Kaaden (1977) illustrated the effects of vibration on the consolidation strength of bulk solids by using a Jenike shear cell fitted with a vibration exciter. They reported that the application of mechanical vibration could significantly enhance the material flow in the hoppers. In an experimental study, Roberts and Scott (1978) found that the strength and the

corresponding flow function of bulk solids were frequency dependent. At some particular frequency, shear strength and flow functions become minimum. Roberts et al. (1986) reported that shear strength of bulk solids decreased exponentially with increases in vibration velocity until the limiting critical state condition was reached. The objective of this chapter is to develop a theoretical model to predict the vibrational energy required to destroy arches in bulk solid storage bins filled with cohesive materials.

7.2. Model Development

7.2.1. Force equilibrium on arch

Arches normally form in the hopper some distance above the discharge outlet. Force equilibrium on an arch is shown in fig. 7.1 for the worst scenario for arch destruction. In this scenario, the arch has no support from the material underneath it, and there is no gravity force acting on the top surface of the arch (Jenike, 1964). The arch is solely supported by shear force S. Under the at-rest condition, the arch-destruction force (F_b) that could break the arch is the weight (W) of arch itself. Therefore, the condition for arch destruction under the at-rest condition is: $F_b = W \geq S$. When the arch is subjected to vibration, the condition for arch destruction becomes (fig.7-1):

$$F_b = (W + F_e) \geq S \tag{7-1}$$

where:

F_b = force to break the arch (N),

F_e = inertial force due to vibration (N),

W = weight of the arch (N), and

S = shear force exerted on the arch (N).

For rectangular hopper outlets, the two components of the arch destructive force are determined as follows:

$$W = BLT\rho g \tag{7-2}$$

$$F_e = BLT\rho \ddot{x} \tag{7-3}$$

where:

$\ddot{x}$ = vibration acceleration of arch (m/s^2),

g = gravitational acceleration (m/s^2),

T = thickness of arch (m),

L = length of arch (m),

B = width of arch (m), and

ρ = bulk density of material (kg/m^3).

Assuming that the stress distribution is uniform within the arch, the stress state at the failure (arch destruction) can be represented by a Mohr circle (fig. 7-2). Therefore, the maximum shear stress is calculated as follows:

$$\tau_{max} = \frac{f_c}{2} \tag{7-4}$$

Where:

τ_{max} = the maximum shear stress in bulk solid comprising no arch (N/m^2), and

f_c = unconfined strength of material (N/m^2).

The shear force is now calculated as:

$$S = \tau_{max} \times A = \left(f_c/2\right) TL \times 2 \tag{7-5}$$

where:

A = area of shear surface (m^2).

7.2.2. Inertial force due to vibration

A motion equation for cohesionless bulk solid systems under vertical vibration was developed in chapter 4. A similarly motion equation can be developed for a cohesive material system if the material is modeled as thin layers connected by elastic and damping elements (fig. 7-3):

$$[M]\{\ddot{x}\} + [C]\{\dot{x}\} + [K]\{x\} = \{F\} \tag{7-6}$$

where:

{x} = displacement vector (m),

$\{\dot{x}\}$ = velocity vector (m/s),

$\{\ddot{x}\}$ = acceleration vector (m/s^2),

[M] = mass matrix,

[C] = damping matrix,

[K] = stiffness matrix, and

{F} = exciting force vector.

A cohesive bulk material is composed of a great number of particles with different sizes. Inter-particle forces may act as damping during vibration. These damping forces can be represented by cohesive proportional damping (Beards, 1983), or mathematically the damping matrix has the form of:

$$[C] = \beta[M] \tag{7-7}$$

where:

β = proportional constant.

Substituting equation (7-7) into (7-6) yields:

$$[M]\{\ddot{x}\} + \beta[M]\{\dot{x}\} + [K]\{x\} = \{F\} \tag{7-8}$$

To solve equation (7-8), a coordinate transformation is performed:

$$\{x\} = [U]\{\eta\} \tag{7-9}$$

where:

[U] = normalized vibration shape matrix, and

$\{\eta\}$ = displacement vector in the normal coordinate system.

The shape matrix [U] represents the eigenvectors normalized with respect to the mass matrix and it may be obtained numerically by applying the inverse superposing method described in chapter 6. The normalized vibration shape matrix has the following characteristics (Timoshenko,1974; Hatter, 1973):

$$\{U\}^T[M][U] = [I] \qquad \text{and} \qquad \{U\}^T[K][U] = [\omega_n^2] \tag{7-10}$$

where:

[I] = unity matrix, and

$[\omega_n^2]$ = diagonal matrix of eigenvalues.

Substituting equation (7-9) into (7-8) yields:

$$[M][U]\{\ddot{\eta}\} + \beta[M][U]\{\dot{\eta}\} + [K][U]\{\eta\} = \{F\} \tag{7-11}$$

Multiplying both sides of equation (7-11) with $[U]^T$ yields:

$$[U]^T[M][U]\{\ddot{\eta}\} + \beta[U]^T[M][U]\{\dot{\eta}\} + [U]^T[K][U]\{\eta\} = [U]^T\{F\} \tag{7-12}$$

The term $[U]^T\{F\}$ represents the exciting force vector in the normal coordinate system and it is denoted as $\{N(t)\}$. Combining equations (7-10) and (7-12) yields:

$$[I]\{\ddot{\eta}\} + \beta[I]\{\dot{\eta}\} + [\omega_n^2]\{\eta\} = \{N(t)\} \tag{7-13}$$

Equation (7-13) represents a set of independent (de-coupled) equations:

$$\ddot{\eta}_i + \beta\dot{\eta}_i + \omega_{ni}^2\eta_i = N_i(t) \qquad (i = 1, 2, \cdots, n) \tag{7-14}$$

where:

$\eta_i, \dot{\eta}_i, \ddot{\eta}_i$ = displacement, velocity, and acceleration along the *i*th normal coordinate respectively,

ω_{ni} = the *i*th natural frequency of system (1/s), and

$N_i(t)$ = exciting force along the *i*th normal coordinate.

If the bin is excited by at single frequency ω at the bottom of the hopper, then the exciting force along the normal coordinate η_i can be represented by:

$$N_i(t) = A_i \sin\omega t \tag{7-15}$$

where:

A_i = amplitude of exciting force along the *i*th normal coordinate,

ω = angular frequency (1/s), and

t = time (s).

For the excitation given by equation (7-15), solutions to equation (7-14) have the form of (Beards, 1983):

$$\eta_i = \frac{A_i}{\omega_{ni}^2 \sqrt{(1 - r_i^2)^2 + (2\xi_i r_i)^2}} \sin(\omega t - \varphi_i) \qquad (i = 1,2, \cdots, n) \qquad (7\text{-}16)$$

where:

r_i = the *i*th frequency ratio ($r_i = \omega/\omega_{ni}$),

ξ_i = the *i*th damping ratio ($\xi_i = \beta / 2\omega_{ni}$), and

φ_i = the *i*th phase angle.

Under the resonant vibration condition (system vibrates at one of the natural frequencies), the damping ratio can be calculated from the ratio of displacement amplitude between the top and bottom layers of the material in the bin by applying the transmissibility calculation formula (Beards, 1983; Timoshenko,1974):

$$\frac{A_T}{A_B} = \sqrt{\frac{1 + 4\xi_i^2}{4\xi_i^2}} \qquad (7\text{-}17)$$

where:

A_T = displacement amplitude of top layer (m), and

A_B = displacement amplitude of bottom layer (m).

At a natural frequency of 33 Hz, an accelerometer was placed on the top free surface of the ground feed to measure the vibration of the top layer and another accelerometer was placed on the bottom base plate to measure the vibration of the bottom layer. When the top displacement amplitudes were measured to be 0.21 mm (standard deviation SD = 0.014), the bottom displacement amplitudes were measured to be 0.048 mm (SD=0.002). This resulted in a damping ratio of 0.12.

To carry out the solution procedure numerically, the stored material needs to be divided into

layers, and the acceleration of each layer is determined from equations (7-16) and (7-9) as follows:

$$\ddot{x}_i = \sum_{j=1}^{n} U_{ij}\ddot{\eta}_j$$

$$= \sum_{j=1}^{n} \frac{-U_{ij}A_j r_j^2}{\sqrt{(1-r_j^2)^2 + (2\xi_j r_j)^2}} \sin(\omega t - \varphi_j) \qquad (i = 1,2, \cdots, n) \tag{7-18}$$

Combining equations (7-1), (7-2), (7-3), and (7-5) results in the following criterion for arch destruction:

$$BLT\rho\left[g + \sum_{j=1}^{n} \frac{-U_{ij}A_j r_j^2}{\sqrt{(1-r_j^2)^2 + (2\xi_j r_j)^2}} \sin(\omega t - \phi_j)\right] > f_c TL \tag{7-19}$$

The acceleration amplitude varies with the frequency (or frequency ratio r_j) and the maximum value of the acceleration amplitude of the ith layer is found by differentiating $\ddot{X}_i$ with respect to r_j:

$$\frac{\partial \ddot{X}_i}{\partial r_j} = 0 \tag{7-20}$$

or

$$\frac{2U_{ij}A_j r_j[(1-r_j^2)^2 + (2\xi_j r_j)^2] + U_{ij}A_j r_j^2[2r_j(1-r_j^2) - 4\xi_j^2 r_j]}{[(1-r_j^2)^2 + (2\xi_j r_j)^2]^{3/2}} = 0 \tag{7-21}$$

A solution to equation (7-21) is: $r_j = \omega/\omega_{nj} \approx 1 (j = 1, 2, \cdots\cdots, n)$, if ξ_i is small. This means that for a specific layer of cohesive material, its maximum acceleration amplitudes occur near specific natural frequencies of the system. If an arch is located in this layer, the optimal vibration frequency for arch destruction is one of the natural frequencies of the storage system. When vibrated at a proper natural frequency, the arch destruction criterion becomes:

$$BLT\rho\left[g + \frac{-U_{ij}A_j}{2\xi_j} \sin(\omega_{nj} t - \phi_j)\right] > f_c TL \tag{7-22}$$

It should be noted that the effect of hopper angle α is not considered in deriving the above criterion. A corrective factor H(α) could be introduced to modify equation (7-22) (Jenike, 1964):

$$\frac{1}{H(\alpha)} = \left(\frac{65}{130+\alpha}\right)^{s}\left(\frac{200}{200+\alpha}\right)^{1-s} \tag{7-23}$$

where:

H(α) = corrective factor,

α = hopper angle (rad),

s= 1 for circular and square openings, and

s = 0 for rectangular opening.

Multiplying the left side of (7-22) by 1/H(α) yields:

$$\frac{BLT\rho}{H(\alpha)}\left[g + \frac{-U_{ij}A_j}{2\xi_j}\sin(\omega_{nj}t - \phi_j)\right] > f_c TL \tag{7-24}$$

If a bin is vibrated at the bottom by a single frequency vibrator, the excitation is applied to the bottom layer of the material stored in the bin. This bottom layer is modeled as the first element in the model and the excitation is expressed as:

$$A_j \sin(\omega_{nj}t - \phi_j) = \{U_j\}^T F = U_{1j} a_v \rho h \sin(\omega_{nj}t - \phi_j) \tag{7-25}$$

where:

$\{U_j\}^T$ = transposed *j*th eigenvector normalized with respect to mass,

F = input inertial force vector exerted by vibrator on unit cross sectional area of cohesive material (N),

a_v = acceleration amplitude supplied by vibrator (m/s^2), and

h = depth of the cohesive material (m).

Substituting equation (7-25) into (7-24) and solving for the required vibration acceleration amplitude a_v for arch destruction gives:

$$a_v > \left|\frac{2\xi_j\left[H(\alpha)f_c / B\rho - g\right]}{U_{ij}U_{1j}\rho h}\right| \tag{7-26}$$

for rectangular hopper outlets, and

$$a_v > \left| \frac{2\xi_j \left[2H(\alpha) f_c / D\rho - g \right]}{U_{ij} U_{1j} \rho h} \right| \tag{7-27}$$

for circular hopper outlets.

where:

D = diameter of outlet opening, (m).

The required thrust force for arch destruction is calculated as:

$$F_v = a_v \rho h S \tag{7-28}$$

where:

h = bin (material) height (m), and

S = bin cross-sectional area (m^2).

7.3. Verification of the Criterion for Arch Destruction

To measure the arch destroying vibration amplitude to verify (7-26), a model hopper-bottomed bin was constructed for conducting the experiment. The cylindrical bin had a diameter of 178 mm and a height of 120 mm. The bin was relative small so that it could be mounted on a vibrator with precise control of vibration frequency and amplitude. A conical hopper of 40° slope and 100 mm height was bolted to the bin. The bin and hopper were both made of 2 mm thick sheet steel. The coefficient of friction between the steel surface and the ground feed used in the experiment was measured as 0.43 by using a direct shear apparatus.

The bin (including the hopper) was mounted on a bench top vibrator (Ling Dynamic Systems 400, Royston, Hertfordshire, England). A Vitec Model 654 CS Mini-Analyzer (Vitec Incorporated, Cleveland, Ohio, USA) was attached to the baseplate of the hopper to measure the displacement amplitude directly. For the following five random selected frequencies 18, 33, 50, 70, and 90 Hz, their corresponding parameters were substituted into criterion (7-27) for verification. Other model parameters are listed in Table 7-1.

The ground feed used in the experiment was a mixture of ground oats and mashed fish bones. A 103 mm inner diameter cylinder with one open end and a 35 mm diameter outlet at the other end was used to determine the yield strength of the feed under a particular consolidation pressures. An

arch layer thickness of 30 mm and 35 mm in diameter was artificially created under a pre-consolidation pressure of 1013 N/m^2. The maximum force required to destroy the arch was 1.58 N averaged over 3 replicates (standard deviation 0.11). This force which acted as a shear force exerted on the perimeter of the arch layer on top of a ground feed cylinder as is shown in fig. 7-4. The area of the vertical section around the perimeter of the circular arch is:

$$S_p = \pi \times D_{arch} \times h_{arch} = 3.14 \times 0.035 \times 0.03 = 3.3 \times 10^{-3} \quad m^2 \qquad (7\text{-}29)$$

where:

S_p = area of the vertical section of the circular arch (m^2),

D_{arch} = diameter of the arch (m), and

h_{arch} = thickness of the arch (m).

Therefore the maximum shear stress is:

$$\tau_{max} = F_s / S_p = 1.58 / 3.3 \times 10^{-3} = 479 \quad N/m^2 \qquad (7\text{-}30)$$

where:

τ_{max} = the maximum shear stress of the arch (N/m^2), and

F_s = exerted shear force (N).

Hence the ultimate strength of the arch was calculated as:

$$f_c = 2 \times \tau_{max} = 2 \times 479 = 958 \quad N/m^2. \qquad (7\text{-}31)$$

Before vibration, the particle and bulk density of theground feed were measured as 1455.1 (kg/m^3) and 469.9 (kg/m^3) averaged over 3 replicates by using an air compression pycnometer. The bulk density of the feed after vibration was measured as 568 (kg/m^3). The water content of the feed was measured as 9.53 % from 3 replicates. The damping ratio of the feed was calculated from the ratio of measured top vibration amplitude and bottom vibration amplitude by using vibration method as described in chapter 8.

In the experiment, the arch was considered to have been destroyed when a continuous flow was observed for more than 30 seconds. The experimental peak acceleration amplitudes at which arches were destructed were calculated from the measured vibration displacement:

$$a_p = \sqrt{2} A \pi^2 f^2 \qquad (7\text{-}32)$$

where:

a_p = peak acceleration amplitudes (m/s^2),

A = measured vibration displacement (effective value) (m), and

f = vibration frequency (Hz).

The comparison between experimental peak acceleration amplitudes for arch destruction and the theoretical criterion for arch destruction is listed in table 7-2. The result shows that the criterion is in good agreement with the measured arch destruction amplitude.

7.4. Conclusions

1. Vibration forces required for destroying arches in storage bins filled with cohesive materials may be predicted by considering the force equilibrium on the arch and vibration characteristics of the storage systems.
2. The optimal vibration frequency for arch destruction is one of the natural frequencies of the cohesive material system.

Table 7-1. Parameters in criterion for calculating arch destruction amplitude

Frequency (Hz)	18	33	50	70	90
Damping ratio (ξ_j)	0.07	0.12	0.18	0.20	0.24
Hopper slope (α)			40°		
Yield strength (f_c, N/m^2)			958		
Diameter of outlet (D, m)			0.01		
Density of ground feed $\rho(kg/m^3)$			568 (after consolidation)		
$U_{ij} \times U_{1j}$	0.94×0.11	1.12×0.20	0.65×0.29	0.61×0.41	1.12×0.53

Table 7-2. Comparison between experimental peak acceleration amplitudes for arch destruction and the theoretical criterion for arch destruction

Frequency (Hz)	Measured vibration displacement (mm)	Experimental peak acceleration amplitudes for arch destruction (m/s_2)	Theoretical criterion for arch destruction (m/s^2)
18	2.36	10.66	10.75
33	0.61	9.28	8.5
50	0.49	17.39	15.3
70	0.09	11.45	12.70
90	0.06	6.78	6.41

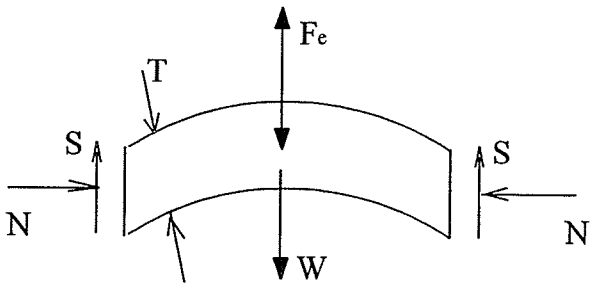

Figure 7-1. Force balance on an arch

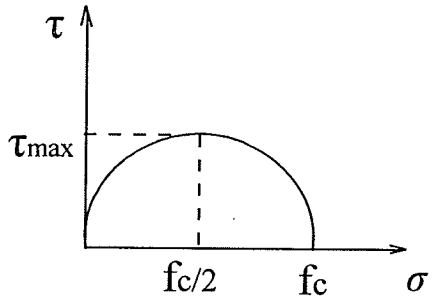

Figure 7-2. Mohr circle for failure state of arch

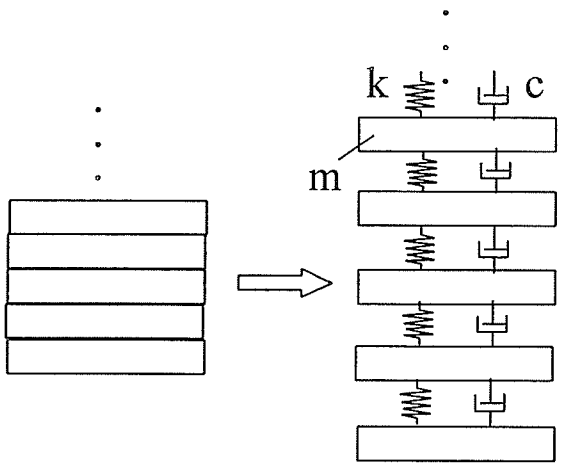

Figure 7-3. Thin layer model for cohesive bulk solids

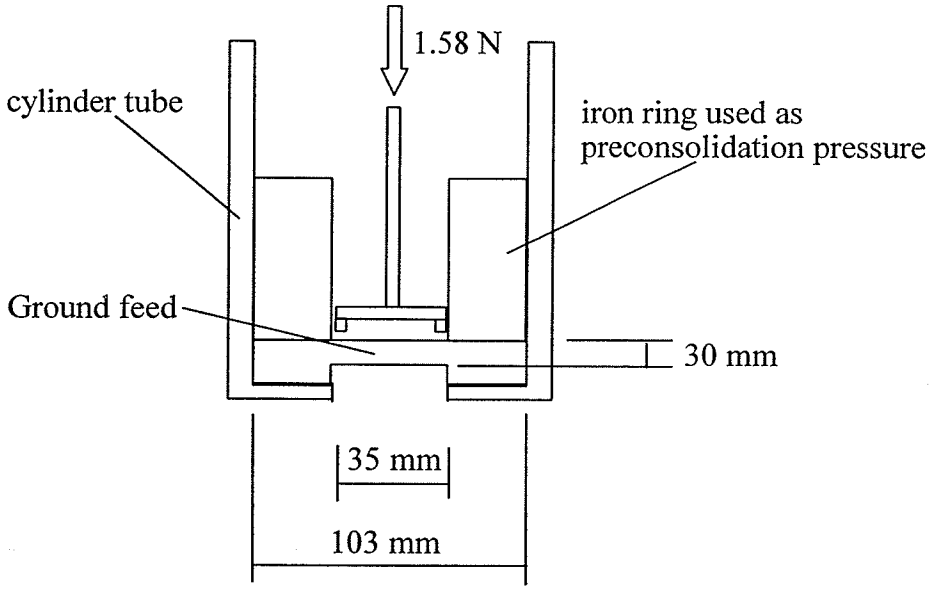

Figure 7-4. Schematic diagram for measuring yield strength of ground feed

Chapter 8. ARCH FORMATION AND DESTRUCTION IN BULK SOLIDS STORAGE BINS DURING VIBRATION

Summary

An experiment was conducted to determine the effect of vibration on formation and destruction of arches in a model bin filled with a cohesive powder (ground feed). The hopper-bottomed bin was 178 mm in diameter and 220 mm high and mounted on a bench top vibrator. Tests were conducted in frequencies from 10 to 200 Hz. When the bin was vibrated the first time, a series of arches formed and were destroyed. As the vibration amplitude was increased, this arch formation-destruction process repeated, the material consolidated, and the location of arch moved upward until a continuous flow occurred. Consolidation strengthened the arches considerably. The vibration amplitude required to destroy the consolidated arches was about 3 times higher than that for non-consolidated arches. The most effective frequencies for arch destruction were near the natural frequencies of the storage system, but not all the natural frequencies were optimal for arch destruction. Those that produced peak inertial forces near the location of the arch were the most effective in destroying the arches.

8.1. Introduction

Arching is one of the most serious flow problems in handling of cohesive bulk solid materials. In storage bins, an arch forms when the stored material develops enough strength to support the bulk solid material above the outlet to stop material flow. Vibration has been studied and used to break arches in storage bins (Roberts et al., 1979; 1986), but with limited success. A dilemma of using vibration for breaking arches is vibration-induced consolidation.

Arch formation is closely related to the yield strength of the cohesive material (Shamlou, 1988). The yield strength is in turn affected by consolidation of the material, that is, consolidation generally leads to higher yield strength. Therefore, if not used properly, vibration may cause stronger arches in storage bins instead of breaking them. To date, little is known about how the vibration affects arch formation and destruction in bulk storage bins.

Bulk solids are discontinuous in nature. When a bulk solid storage bin is subjected to vibration, different vibration frequencies and modes may exist at different locations. To break an

arch in the bin, vibrating energy should be directed to where the arch is located. In other words, only certain vibration frequencies and modes would be effective in breaking arches. The objective of this study was to determine the relationship between the vibration characteristics and arching behavior (arch formation and destruction) in a model bin filled with cohesive ground feed.

8.2. Methodology

The same model hopper-bottomed bin as described in Chapter 7 was used in the experiment. The bin (including the hopper) was mounted on a bench top vibrator (Ling Dynamic Systems 400, Royston, Hertfordshire, England) (fig. 8-1). The system was capable of providing vibration frequencies from 0 to 9 kHz, and a maximum thrust force of 196 N. An accelerometer (Model 4366, B&K Ltd., Nærum, Denmark) was attached to the baseplate of the model bin to measure the vibration acceleration. Acceleration signals were amplified by a conditioning amplifier (Model 2626, B&K Ltd.) and analyzed by an oscilloscope (Model 2090-III, Nicolet Instrument Corporation, Madison, Wisconsin, USA). Another vibration analyzer (Model 654 CS, Vitec Inc., Cleveland, Ohio, USA) was also attached to the baseplate to measure the displacement amplitude directly.

Ground feed was tested in the experiment. The moisture content of the feed was 9.5 % wet basis. The particle density was 1455 kg/m^3 as measured by using an air compression pycnometer. The bulk density before vibration was 470 kg/m^3. The internal friction coefficient was determined as 0.73 by using a direct shear apparatus and by adopting the same procedure as Inglis (Inglis, 2001).

Preliminary tests were conducted to determine a proper hopper opening to "create" arches in the hopper. It was found that flow could not be initiated without vibration when the hopper opening was less than 10 mm. Therefore, a 10-mm opening was used in all tests. Once the opening was determined, another set of preliminary testes were conducted to determine the range of vibration frequency to be used. The bin was filled and vibrated at frequencies between +0 to 9 kHz. At each frequency, the vibration amplitude was increased gradually until a continuous flow was observed. This amplitude was recorded as the arch destruction vibration amplitude (ADVA). It was found that arches could not be destructed at any amplitude when the frequency was lower than 10 Hz, whereas, the vibrator could not provide enough thrust (the limit was 196 N) to break arches when the frequency was higher than 200 Hz. Therefore, the frequency range from 10 to 200 Hz was used in the subsequent tests.

In the first series of tests, ADVAs were measured as a function of frequency. The tests were conducted in the 10 - 40 Hz range at 3 Hz increment, 40-50 Hz range at 5 Hz increment, 50-160 Hz range at 10 Hz increment, and 160- 200 Hz range at 20 Hz increment. For each test (frequency), the feed was stream filled into the bin through a large filling hopper located 100 mm above the bin and the feed surface was leveled with a ruler. After 5 minutes of settling, the discharge gate was opened to let a small amount of material to flow out. This small amount of material was between the discharge gate and the arch. When the flow stopped, a ruler was used to measure the arching height (the distance between the arch and the outlet). The vibration amplitude was then increased gradually until the arch was broken. To consider the combined effect of frequency and amplitude, the inertial force for arch destruction (IFAD) was calculated:

$$F_A = 4\pi^2 f^2 A \tag{8-1}$$

where:

F_A = inertial force for arch destruction (IFAD) per unit mass (N/kg),

f = vibration frequency (Hz), and

A = vibration (displacement) amplitude for arch destruction (ADVA) (m).

In the second series of tests, a frequency (33 Hz) that was the most effective in destroying arches was selected for bin vibration and the material consolidation was measured. The vibration amplitude was increased incrementally from 0.05 mm to ADVA. At each amplitude increment, the bin was vibrated until the maximum consolidation was achieved. Each test condition was replicated three times.

8.3. Results and Discussion

8.3.1. Arch formation and destruction during vibration

An initial arch formed and the flow stopped when a small amount of material between the discharge gate and the arch was emptied out of the bin. This initial arch was located slightly above the discharge opening. The initial arch was broken when the vibration amplitude reached a certain level. However, a new arch formed subsequently at a higher location. This arch formation-destruction cycle continued as the amplitude was increased gradually, and the arch location moved upward as the cycle continued. For example, seven arches formed and were destroyed before a

continuous flow began for a test conducted at 33 Hz. The arch location moved from ~0 (initial) to ~25 mm (final) above the discharge outlet (fig. 8-2). It should be noted that the measurement of arch location was accurate to ± 2 mm. The last arch that was destroyed before continuous flow was termed the primary arch in the following discussion. A similar process was observed for other frequencies and the results of ADVAs and final arch locations are summarized in Table 8-1.

As the vibration amplitude was increased, material consolidation increased until the vibration amplitude reached a certain value that caused the material to flow continuously. Figure 8-3 shows this consolidation process for a test conducted at 33 Hz. In this particular example, the material was consolidated 17% (26 mm settlement) before a continuous flow started. Results for other frequencies are shown in Table 8-1.

A secondary arch formed when the vibrator was turned off. This secondary arch was destroyed with a much lower vibration amplitude when the vibrator was re-started (Table 8-1). For example, the amplitude for the destruction of the secondary arch was 0.17 mm, or 30% of that for the primary arch, for the 33 Hz tests. This meant that consolidation considerably increased the arch strength. The primary arch was the last one to be broken before the continuous flow started, therefore, it was subjected to the most consolidation during the arch formation-destruction cycle. Whereas, the secondary arch was not subjected to the arch formation-destruction cycle and it was destroyed before very much consolidation took place.

The vibration amplitude for arch destruction decreased sharply with the vibration frequency when the frequency was below 25 Hz and it changed little when frequencies were higher than 33 Hz (fig. 8- 4). This was because there was more vibrating energy transferred into the system at higher frequencies, thus smaller amplitudes needed to destroy arches. To examine the combined effect of vibration amplitude and frequency, the inertial force for arch destruction (IFAD) was plotted in figure 8-4. The curve had a skewed "U" shape, with the two lowest IFAD values at 33 and 90 Hz. In other words, the minimum vibrational energy was needed to destroy an arch if the bin was vibrated at 33 or 90 Hz for the test bin used in this study. Therefore, for each storage system, there may exist frequencies that are the most effective for arch destruction. To further examine the most effective arch destruction frequencies, numerical simulations were performed.

8.3.2. Numerical simulations

Simulations were based on a model developed in Chapter 7. The governing equation had the form of:

$$[M]\{\ddot{x}\} + [C]\{\dot{x}\} + [K]\{x\} = \{F\} \quad (8\text{-}2)$$

where:

[M] = mass matrix,

[C] = damping coefficient matrix,

[K] = stiffness matrix,

x = vibration displacement (m),

{F} = excitation (N),

.. = second derivative with respect to time, and

. = first derivative with respect to time.

The required model parameters for simulations are those in the mass, damping and stiffness matrices. The mass matrix is defined as: M_{ij} = unit mass for i=j; and M_{ij} = 0 for i≠j. In the simulations, the material was divided into layers of 2.5 mm and each layer with a unit area (1 m^2) represented the unit mass. Therefore, the unit mass was calculated to be 1.42 kg/m^2, as the product of the bulk density and the layer thickness.

Based on the vibration theory (e.g., Beards, 1983; Timoshenko,1974), the damping coefficient C_{ij} is dependent on the damping ratio ξ_i:

$$C_{ii} = 2M_{ii}\omega_{ni}\xi_i \quad \text{and} \quad C_{ij} = 0 \quad \text{for} \quad i \neq j \quad (8\text{-}3)$$

where:

C_{ij} = element of damping coefficient matrix (Ns/m),

M_{ii} = element of mass matrix (kg),

$\omega_{n\,i}$ = the *i*th natural frequency (1/s), and

ξ_i = damping ratio.

The parameter that defines the stiffness matrix [K] is the equivalent inter-layer stiffness (k_A) of the bulk solids:

$$[K] = k_A \begin{bmatrix} 1 & -1 & 0 & \dots \\ -1 & 2 & -1 & \dots \\ 0 & -1 & 2 & \dots \\ \dots & \dots & \dots & \dots \end{bmatrix} \quad (8\text{-}4)$$

The coefficient k_A was determined from the consolidation data measured in 33 Hz tests. The maximum consolidation was measured to be 26 mm before a continuous flow occurred and the corresponding vibration amplitude was 0.61 mm (Table 8.1). The compression ratio of the material (R_c) was therefore calculated as:

$$R_c = (\text{consolidation}) \div (\text{total material height}) = 26 \div 220 = 0.12 \quad (8\text{-}5)$$

This compression ratio was caused by the thrust force F_A expressed per unit cross sectional area:

$$F_A = m_s a = \rho LA\omega^2 = 4\rho LA\, f^2 \pi^2 \quad (8\text{-}6)$$

where:

F_A = inertial force per unit cross-sectional area of material layer (N/m^2),

m_s = material mass per unit cross-sectional area of material layer (kg/m^2),

a = vibration acceleration of material (m/s^2),

ρ = bulk density of material (kg/m^3),

L = height of the material above the arch (m), and

ω = angular frequency (1/s).

On the other hand, this inertial force was balanced by an elastic force as the material layer is compressed. For a material layer with a thickness of x, this elastic force is:

$$F_e = k_D \Delta x = k_A R_c x \quad (8\text{-}7)$$

where:

k_D = equivalent dynamic inter-layer stiffness (N/m), and

x = layer thickness (m).

Equating equations (8-6) and (8-7), and then solving the resulting equation for k_A:

$$k_D = Fe/R_c x = F_A/R_c x = 4\rho LA\, f^2 \pi^2 /(R_c x) \quad (8\text{-}8)$$

Substituting known parameter values into equation (8-8), the equivalent unit area inter-layer rigidity k_D was calculated to be:

$$k_D = 568\times0.1685\times(4\times0.17\times10^{-3})\times33^2\times\pi^2 / (0.12\times2.5\times10^{-3}) = 2.13\times10^6 \text{ N/m} \quad (8\text{-}9)$$

It is proved theoretically in Chapter 7 that the minimum vibrational forces were required to destruct arches if the bin was vibrated at one of its natural frequencies. The model predicted 27 natural frequencies in a range from 3.8 to 200.7 Hz by applying the inverse superposition algorithm developed in Chapter 6. Both 33 and 90 Hz were near a predicted natural frequency: 33 (measured) vs. 34.4 Hz (predicted); and 90 (measured) vs. 94.8 Hz (predicted). It was clear that not all the natural frequencies were optimal for arch destruction because the maximum vibration force might not occur at the location where the arch existed even though the bin was vibrated at a natural frequency. This concept is illustrated in figure 8-5, which shows the simulated vibration amplitude at a natural frequency of 34.4 Hz. It can be seen that the maximum vibration amplitude occurred at distances (above the outlet) of 23, 68, 113 mm, and so on. In the experiment, the arch was measured at 25 mm above the outlet (Table 8-1). This indicates that when the bin was vibrated at 33 Hz, the maximum vibrational force occurred near the arch. In other words, the 34.4 Hz was an optimal frequency for arch destruction in the test bin. To search for additional optimal frequencies, the locations of the first and second peaks of vibration amplitude for other natural frequencies are plotted in figure 8-6. The higher peaks were not plotted because they occurred in the upper part of the bin, and thus had little effect on arches. A C++ code was developed to select the optimal vibration frequencies for arch destruction (Appendix D). The two natural frequencies that produced peak amplitudes near the arch location (25 mm) were 34.4 and 94.8 Hz. This explains why 33 and 90 Hz corresponded to the lowest vibrational force needed for arch destruction.

8.4. Conclusions

1. A series of arches formed and were destroyed during the initial vibration. The location of the arch moved upward in the hopper as the arch formation-destruction cycle proceeded. A continuous flow occurred when the vibration amplitude reached a certain value.
2. Consolidation increased the strength of arches. The vibration amplitude required to destroy the primary (consolidated) arches was about 3 times higher than that for secondary (non-consolidated) arch.
3. The most effective frequencies for arch destruction were near the natural frequencies of the storage system, but not all the natural frequencies were optimal for arch destruction. Only

those that produced peak inertial forces near the location of arch were effective in destroying the arch.

Table 8-1. Measured vibration (displacement) amplitudes for arch destruction, arch locations, and vibration-induced consolidation

	Amplitude for Destroying Primary Arch (mm)	Arch Location (mm)	Material Settlement (mm)	Amplitude for Destroying Secondary Arch (mm)
18 Hz	2.36 (0.128)	23-27	24-26	0.84 (0.062)
33 Hz	0.61 (0.015)	23-27	25-27	0.17 (0.028)
90 Hz	0.06 (0.001)	23-27	22-24	0.02 (0.003)

( ) is the standard deviation of the measured data.

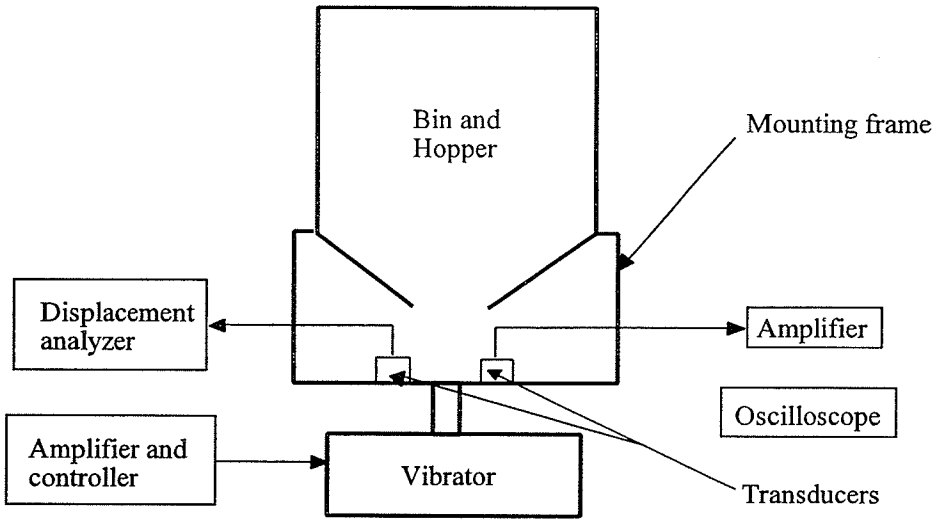

Figure 8-1. Schematic illustration of model bin test setup

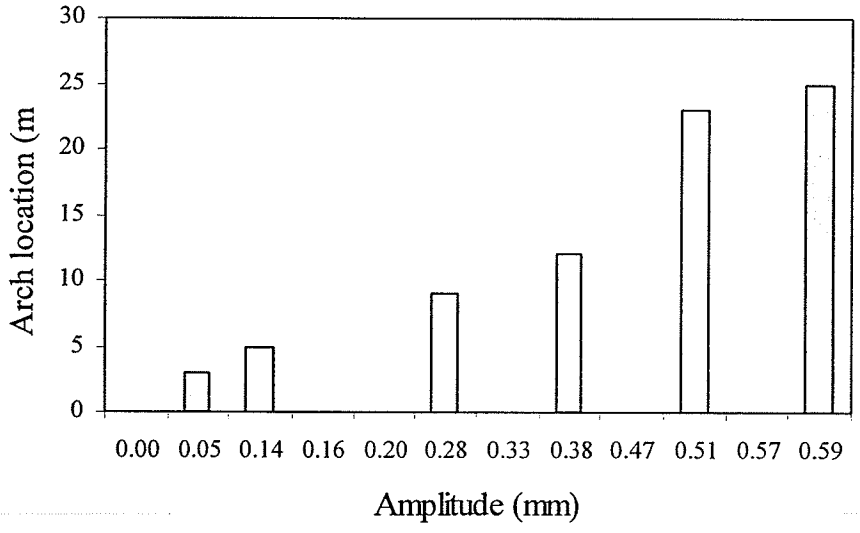

Figure 8-2. Arch locations during initial vibration

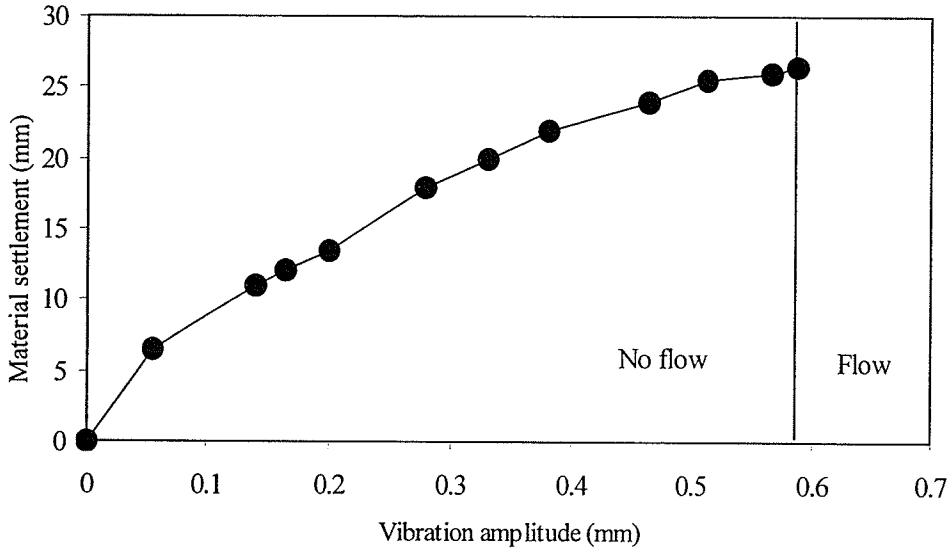

Figure 8-3. Material consolidation during vibration

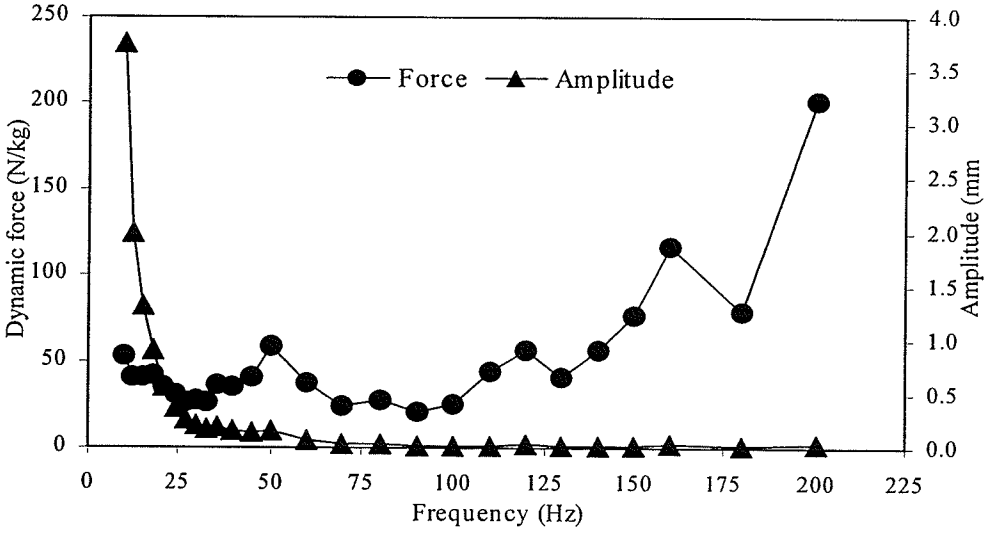

Figure 8-4. Displacement amplitudes and inertial forces for arch destruction

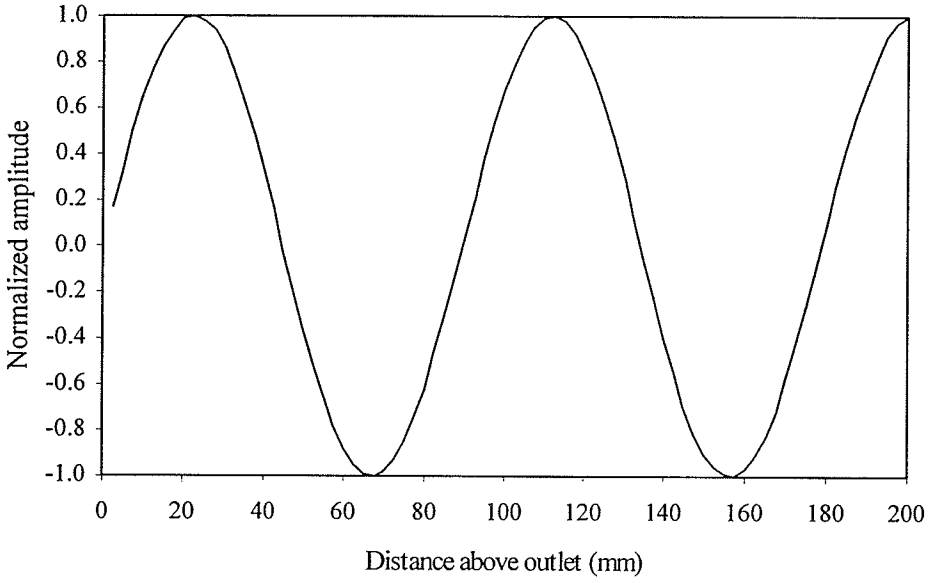

Figure 8-5. Simulated vibration peaks for a natural frequency of 34.4 Hz

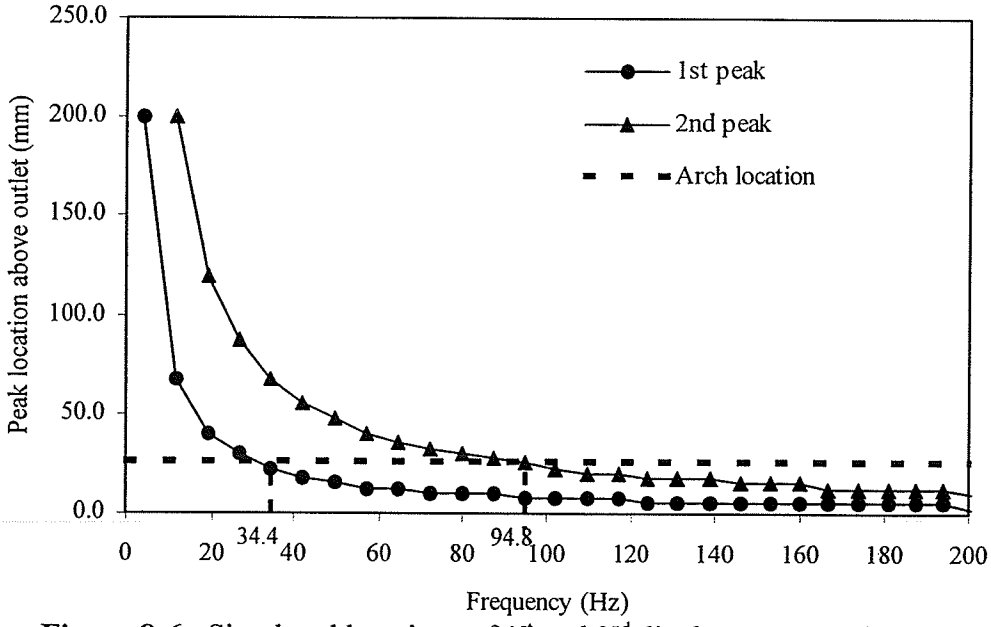

Figure 8-6. Simulated locations of 1st and 2nd displacement peaks

Chapter 9. CONCLUSIONS

1. The vertical vibration of grain storage bins was adequately modeled by a one-dimensional spring-damper system. The model prediction of grain settlement (consolidation) was in good agreement with the experimental data for a model bin. The calculated values of overall average differences were 17%, 8% and 11% for 23, 30 and 48 Hz tests, respectively.
2. For the range of frequency (23, 30, and 48 Hz) tested, the grain reached its maximum bulk density (theoretic limit) at different amplitudes. The higher the frequency, the lower the amplitude at which the maximum density (consolidation) occurred. The maximum density was independent of the vibration frequency.
3. The rate of consolidation within the grain mass increased with the grain depth in a nonlinear fashion. Both the amplitude and frequency affected the variation of grain consolidation with the grain depth. A higher amplitude or frequency would result in a quicker increase of grain settlement (consolidation) with the grain depth.
4. The numerical model developed in this study adequately predicted the increases in lateral pressures induced by vertical vibration. The difference between the predicted pressures and those reported in the literature were less than 12%.
5. The predicted vibration-induced pressure was not uniform in the bin. For a 1.5 m height model bin, the greatest increase in lateral pressure after vibration was 2.2 times the static pressure calculated by Janssen's equation near the bin bottom. For a full size bin with 4 m in diameter and 6 m in height, the predicted vibration-induced pressure had a similar wavy shape as for a 1.5 m height model bin. The lateral pressure for the full size bin predicted by the numerical model is about 50% larger than Janssen's value.
6. Vibration energy has the most significant influence on the predicted lateral pressure. The more vibration energy, the greater the increase in lateral pressure. Vibration frequency has slight effect on lateral pressure. Higher frequency will increase the predicted lateral pressure slightly.
7. A series of arches were formed and destroyed during the initial vibration. The location of arch moved upward in the hopper as the arch formation-destruction cycle proceeded. A continuous flow occurred when the vibration amplitude reached a certain value.

8. Vibration induced consolidation increased the strength of arches. The vibration amplitude required to destroy the primary (consolidated) arches was about 3 times higher than that for secondary (non-consolidated) arches.

9. The most effective frequencies for arch destruction were near the natural frequencies of the storage system, but not all the natural frequencies were optimal for arch destruction. Only those that produced peak inertial forces near the location of arch had the greatest input in destroying the arch.

REFERENCE

ACI. 1983. Recommended practice for design and construction of concrete bins, silos, and bunkers for storage of granular materials. Revised 1983, and commentary. ACI 313R-77. American Concrete Institute, Detroit, MI, USA.

Arnold, P. C. and A. S. Kaaden. 1977. Reducing wall friction by mechanical vibration. *Powder Technology* 16(1):63-66.

Beards, C.F. 1983. *Structural Vibration Analysis: Modeling, Analysis and Damping of Vibrating Structures*, 1st ed. Chichester, West Sussex, England: Ellis Horwood Ltd.

Carroll, J. I. And H. Colin. 1975. Vibrations in solids flow. *Chemical Engineering Progress* 71(2): 53-65.

Craig, R. F. 1997. Soil Mechanics. 6th ed. London; New York: E & FN Spon.

Davies, A.J. 1980. *The Finite Element Method: A First Approach*, New York, NY: Oxford University Press.

Drescher, A. 1991. Analytical Methods in Bin-load Analysis. New York, NY: Elsevier Science Publication Company Inc.

Drescher, A., A.J. Waters, and C.A. Rhoades. 1995. Arching in hoppers: I. Arching theories and bulk material flow properties. *Power Technology* 84(2): 165-176.

Ersov, L. V., and A. A. Lisin. 1964. Method to improve operations of bunker plants. *Teploenergetika* 11:44-47.

Gaylord, Edwin H. Jr., and Charles N. Gaylord. 1984. Design of Steel Bins for Storage of Bulk Solids. Englewood Cliffs, NJ: Prentice-Hall Inc.

Ge, T., Q. Zhang, and M.G. Britton. 1999. Derivation of a theory for predicting consolidation of bulk solids induced by vertical vibration. Paper No. MBSK99-114, presented at the 1999 North-Central Inter-Sectional ASAE & CSAE conference, Winnipeg, Manitoba, Canada.

Ge, T., Q. Zhang, and M. G. Britton. 2000. The effect of vibration frequency and amplitude on grain settlement in a model bin. ASAE paper No. 004009. St. Joseph, MI: ASAE.

Giunta, J.S. 1969. Flow patterns of granular materials in flat-bottom bins. *Transactions of the ASME* 91(5): 406-413.

Grossman, R. B., H. L. Towne, and T. V. Vogel. 1990. Bulk feed bin challenges. ASAE Paper

90-4013. Joseph, MI: ASAE.

Hao, D. 1992. Effect of moisture content of stored grain and vibration on dynamic loads during discharge in a corrugated steel model bin. Unpublished M.Sc. thesis. Department of Biosystems Engineering, University of Manitoba, Winnipeg, MB.

Hao, D., Q. Zhang and M.G. Britton. 1994. Effect of Vibration on Loads in a Corrugated Model Grain Bin. *Canadian Agricultural Engineering.* 36(1): 29-35.

Hatter D. J. 1973. Matrix Computer Methods of Vibration Analysis. Essex, England: Butter worth & Co Ltd.

Inglis, D. H. 2001. Determination of the Coefficient of Friction of Canola. Unpublished B. Sc. thesis. Department of Biosystems Engineering, University of Manitoba, Winnipeg, MB.

Janssen, H. A. 1895. Versuche über getreidedruck in silozellen. Zeitschriff des Vereines Deutscher Ingenieure, 39: 1045-1049.

Jenike, A. W. 1964. Storage and flow of bulk solids. Bulletin No. 123. Utah Engineering Experiment Station, University of Utah, Salt Lake City, Utah.

Jenike, A. W., and J. R. Johanson. 1969. On the theory of bin loads. *Transactions of the ASME* 91(2):339-344.

Jenike, A. W., and J. R. Johanson., and J. W. Carson. 1973. Bin loads — Part 2: Concepts. *Journal of Engineering Industry* 95(1): 1-5.

Jenike, A. W., and T. Leser. 1964. A flow no flow criterion in gravity flow of powders in converging channels. *Procedings of the Fourth Congress on Rheology*, 125-141.

Jofriet, J.C., S.C. Negi and Z. Lu. 1997. A numerical model for flow of granular materials in silos. Part 3:Parametric study. *Journal of Agricultural Engineering Research* 68: 237-246.

Johanson, J. R., and A.W. Janike. 1962. Stress and velocity fields in the gravity flow of bulk solids. *Utah Engineering Experimental Station Bulletin* 53(116).

Johanson, J. R. 1966. The use of flow-corrective inserts in bins. *Transactions of the Society of Mining Engineers* 224-230.

Johanson, J. R. 1967. The placement of inserts to correct flow in bins. *Power Technology* 1:328-333.

Kmita, J. 1991. An experimental analysis of internal silo loads. *Bulk Solids Handling* 11: 459-468.

Kvapil, R. and T. Tanaka. 1965. Bins and bunkers with shield inserts. *Aufber Techn* 6:45-49.

Lu, Z., S.C. Negi and J.C. Jofriet. 1997. A numerical model for flow of granular materials in silos. Part 1: Model development. *Journal of Agricultural Engineering Research* 68: 223-229.

Meng, Q., J.C. Jofriet and S.C. Negi. 1997a. Finite element analysis of bulk solids flow: Part 1, Development of a model based on a secant constitutive relationship. *Journal of Agricultural Engineering Research* 67: 141-150.

Meng, Q., J.C. Jofriet and S.C. Negi. 1997b. Finite element analysis of bulk solids flow: Part 2, Application to a parametric study. *Journal of Agricultural Engineering Research* 67: 151-159.

Moriyama, R., and T. Jotaki. 1980. An investigation of wall pressures in flowing and static bulk materials in model bins. Proceedings of International Conference on Design of Silos for Strength and Flow. University of Lancaster, Lancaster, England.

Myers, J. I. 1970. Vibrating Hoppers. *Journal of Mechanical Engineering* 3:27-31.

Negi, S.C., Z. Lu and J.C. Jofriet. 1997. A numerical model for flow of granular materials in silos. Part 2: Model validation. *Journal of Agricultural Engineering Research* 68: 231-236.

Rappen, A. and H. Wright. 1983. In *Proceedings of the 2nd International Conference on Design of Silos for Strength of Flow* 423-434. Powder Advisory Centre, London.

Richard, A. Link and Alaa E. Elwi. 1990. Incipient flow in silo-hopper configurations. *Journal of Engineering Mechanics* 116(1): 172-188.

Roberts, A. W. and O. J. Scott. 1978. An investigation into the effects of sinusoidal and random vibrations on the strength and flow properties of bulk solids. *Powder Technology* 21:45-53.

Roberts, A. W., O. J. Scott, and Li Kin Wah. 1979. The influence of mechanical vibrations on the strength of flow properties of bulk solids. *International Powder and Bulk Solids Handle and Process, Proceedings of the Technology Program. 445-458.*

Roberts, A. W., M. Ooms, and O. J. Scott. 1986. Influence of vibrations on the strength and boundary friction characteristics of bulk solids and the effect on bin design and performance. *Bulk Solids Handling.* 6(1):161-169.

Rong, G.H., S.C. Negi and J.C. Jofriet. 1995a. Simulation of flow behaviour of bulk solids in bins. Part 1:Model development and validation. *Journal of Agricultural Engineering Research* 62: 247-256.

Rong, G.H., S.C. Negi and J.C. Jofriet. 1995b. Simulation of flow behaviour of bulk solids in bins. Part 2:Shear bands, flow corrective inserts and velocity profiles. *Journal of Agricultural Engineering Research* 62: 257-269.

Savage, S.B. and D.J. Jeffrey. 1981. The stress tenser in a granular flow at high shear rates. *Journal of Fluid Mechanics* 110: 255-272.

Shamlou, P. A. 1988. Handling of bulk solids: *Theory and Practice*. Essex, England: Butterworth & Co Ltd.

Smith, D. L. O., and R. A. Lohnes. 1980. Grain silo overpressures induced by dilatancy upon unloading. ASAE Paper No. 80-3013. St. Joseph, MI: ASAE.

Steidel Jr. R.F. 1979. An introduction to mechanical vibrations. New York, NY: John Wiley and Sons.

Suzuki, A. and T. Tanaka. 1972. Flow of cohesive solids from vibrating hoppers. *Power Technology* 6: 301-308.

Tardos, G.I. and Q. Lu. 1996. Precision dosing of powders by vibratory and screw feeders: an experimental study. Advanced Powder Technology 7(1):51-58.

Timoshenko, S., D. H. Young, and W. Weaver, Jr. 1974. Vibration problems in engineering. New York, NY: John Wiley and Sons.

Visen, N. S.. 1997. Numerical modeling of the effects of bin inserts on stress distribution in storage bins for cohesive powder material. Unpublished M.Sc. thesis. Department of Biosystems Engineering, University of Manitoba, Winnipeg, MB.

Walker, D. M., and M. H. Blanchard. 1967. Pressures in experimental coal hoppers. *Chemical Engineering Science* (22): 1713-1745.

Wes, G.W.J., S. Stemerding and D.J. van Zuilichem. 1990. Control of flow of cohesive powders by means of simultaneous aeration and vibration. Powder Technology 61(1)39-49.

Williams, J. C., J. M. Head, and J. J. Ahumada. 1983. In *Proceedings of the 2nd International Conference on Design of Silos for Strength of Flow* 401-423. Powder Advisory Centre, London.

Xu, S., Q. Zhang and M.G. Britton. 1993. Effect of vibration on stress-strain behavior of wheat en masse. ASAE Paper No. RRV-93-202. St. Joseph, MI: ASAE.

Xu, S., Q. Zhang and M.G. Britton. 1993. Effect of grain dilatancy on dynamic loads in grain bins. ASAE Paper No. 93-4504. St. Joseph, MI: ASAE.

Xu, S., Q. Zhang and M.G. Britton. 1996. A microscopic theory for predicting loads in storage bins for granular materials. *Journal of Agricultural Engineering Research* 65: 253-259.

Yoshida Jun. 1996. Anumerical study on convection of particles in a bin during vertical vibration. *Advanced Powder Technology* 7(4):305-317.

Zhang, Q. M.G. Britton, and J. M. Leitgeb. 1993. Thermally induced pressures in an on-farm grain storage bin. *Journal of Canadian Agricultural Engineering* 35(1): 51-55.

Appendix A. FORTRAN CODE FOR CALCULATION OF CONSOLIDATION

```
c**********************************************************************
      integer i,j
      real mass(6000), damp(6000), stiff(6000,6000), tem1(6000)
      real fi, sita, loo, g, pi, ke, le, fd1, fd2
      real freq1,y0,stif,n1,csoli
      complex ampl(6000), comp1, comp2, ima
c ----- define φ, θ, g, ρ, and π.
      fi=3.14159*25.2/180.0
      sita=3.14159*57.8/180.0
      g=9.8
      loo=797.57
      pi=3.14159
      open(30, file='dcom.dat', status='new')
      open(40, file='acosoli2.dat', status='new')
c ----- ima: unit imaginary number, n1: layer number, freq1= frequency,
c ----- comp1= frequency in compound number, ke = rigidity of bulk grain,
c ----- y0 = height of grain mass, ampl(i) = vibration amplitude of ith layer,
      ima=(0.0,1.0)
      n1=60.0
      freq1=3.14159*2*23
      comp1=(0.0,144.513)
      ke=6.63e5
      y0=0.292
      le=y0/n1
      stif=2.0*ke*sin(sita)*sin(sita)
      ampl(1)=(0.0003687,0.0)
```

```
c ----- fd1 and fd2 : damping
        fd1=loo*g*le*tan(fi)*sin(2*sita)
        fd2=freq1*freq1*loo*le*ampl(1)
        if (fd1 .gt. fd2) then
        damp(1)=fd2
        else
        damp(1)=fd1
        end if
        do 10 i=1, n1
                mass(i)=le*loo
        do 20 j=1, n1
                if (i .eq. 1) then
                        if (j .eq. 1) then
                                stiff(i,j)=stif
                        else if (j .eq. 2) then
                                stiff(i,j)=-stif
                        else
                                stiff(i,j)=0.0
                        end if
                else if (i .eq. n1) then
                        if (j .eq. (n1-1)) then
                                stiff(i,j)=-stif
                        else if (j .eq. n1) then
                                stiff(i,j)=stif
                        else
                                stiff(i,j)=0.0
                        end if
                else
```

```
            if (j .eq. (i-1)) then
                    stiff(i,j)=-stif
            else if (j .eq. i) then
                    stiff(i,j)=2*stif
            else if (j .eq. (i+1)) then
                    stiff(i,j)=-stif
            else
                    stiff(i,j)=0.0
            end if
        endif
5       format(2x, f20.8, 2x, f20.8, 2x, f20.8)
20      continue
10      continue
        print 5, mass(1), damp(1)
        comp2=(comp1*comp1*mass(1)+stif)*ampl(1)+ima*damp(1)
        ampl(2)=comp2/stif
        print 5, ampl(2)
        do 30 i=2, (n1-1)
            fd1=loo*g*i*le*tan(fi)*sin(2*sita)
            fd2=freq1*freq1*loo*le*ampl(i)
            if (fd1 .gt. fd2) then
                    damp(i)=fd2
            else
                    damp(i)=fd1
            end if
        comp2=(comp1*comp1*mass(i)+2*stif)*ampl(i)+ima*damp(i)
        ampl(i+1)=(comp2-stif*ampl(i-1))/stif
30      continue
        print 5, ampl (n1)
```

```
      csoli=0.0
      do 50 i=1, (n1-1)
            tem1(i)=abs(ampl(i+1))-abs(ampl(i))
            write(30,*) abs(tem1(i))
50    continue
      do 60 i=1, (n1-1)
            j=n1-i
            csoli=csoli+abs(tem1(j))
            write(40,*) csoli
60    continue
      tem1(n1)=abs(ampl(n1))-abs(ampl(n1-1))
      write(30,*) abs(tem1(n1))
      write(40,*) csoli
      close(30)
      close(40)
      end
c**********************************************************************
```

Appendix B. C++ CODE FOR CALCULATING LATERAL PRESSURES OF BINS SUBJECTED TO VIBRATION

B.1. C++ code for calculating Janssen's lateral pressure

```
#include<iostream>
#include<fstream>
#include<math.h>

double lp1(double y);

int main()
{
        double y0=6.0;          //height of grain mass
        int n=30;               //number of layers
        double ave=0.0;         //initializing average values

        ofstream fout;
        fout.open("lp10m.dat");

        for(int i=0;i<n;i++)
        {
                double y=y0*(i+1)/n;
                fout<<lp1(y)<<endl;             //lp1(y) = Janssen's value
                ave=ave+lp1(y);
        }
        ave=ave/30.0;
```

```
        cout<<ave<<endl;
        cout<<"calculation finished"<<endl;
        return(0);
}

double lp1(double y)
{
        double loo=797, R=1.0, g=9.8, miu=0.43;
        double e=2.71828, ka=0.403;
        double lpr;
        lpr=exp(-(ka*miu*y/R));
        lpr=loo*R*g/miu*(1-lpr);
        return(lpr);
}
```

B.2. C++ code for calculating total lateral pressure (including vibration induced lateral pressure)

```
#include<iostream>
#include<fstream>
#include<string>
#include<math.h>
#include<cassert>

const int n=30;                 //number of layers
const double depth=6;           //depth of grain mass
const double h=depth/n;         //location above bottom of grain mass
const double ke=6.63e5;         //rigidity of bulk mass
const double loo=797.0;         //bulk density
```

```
int main()
{
// dh[n] = consolidation of the nth layer; lp1[n] = Janssen's value of the nth layer;
// lp1[n] = vibration increased lateral pressure of the nth layer;
// lp[n] = total lateral pressure of the nth layer;
// s1 = cross-sectional area of the bin; s2 = projected ring area on the bin wall of a layer;
        double dh[n], lp1[n] ,lp3[n], lp[n];
        double s1, s2, lps3[n];
        string icname, ilp1name;
        cout<<"enter consolidation input file name:"<<endl;
        getline(cin, icname);
        cout<<"enter 'Janssen's' lateral pressure input file name:"<<endl;
        getline(cin, ilp1name);
        ifstream fin1(icname.data());
        assert(fin1.is_open());
        ifstream fin2(ilp1name.data());
        assert(fin2.is_open());

        string olpname, olp3name, olps3name;
        cout<<"enter elastic compression pressure output filename:"<<endl;
        getline(cin, olp3name);
        ofstream fout3(olp3name.data());
        assert(fout3.is_open());
        cout<<"enter sum of lp1 & lp3 output file name:"<<endl;
        getline(cin, olps3name);
        ofstream fouts3(olps3name.data());
        assert(fouts3.is_open());
        cout<<"enter Janssen's pressure output file name:"<<endl;
        getline(cin, olpname);
```

```
ofstream fout(olpname.data());
assert(fout.is_open());

for(int i=0; i<n; i++)
{
        fin1>>dh[i];
        fin2>>lp1[i];
        double pv, yi, alfa;

        yi=h*i;
        pv=loo*yi;
        alfa=57.8*3.14/180;
        s1=3.14*2*2;
        s2=3.14*4*h;
        lp3[i]=ke*dh[i]*s1*sin(alfa)*cos(alfa)/s2;
        lps3[i]=lp1[i]+lp3[i];
}

double sum=0.0;
for(int i=29; i>-1; i--)
{
        fout3<<lp3[i]<<endl;
        fouts3<<lps3[i]<<endl;
        sum=sum+lps3[i];
        fout<<lp1[i]<<endl;
}
cout<<sum<<endl;

fin1.close();
```

```
//      fout.close();
        fout3.close();
        return(0);
}
```

Appendix C. C++ CODE FOR EIGENVALUES AND EIGEN-VECTORS OF A BULK SOLID SYSTEMS

```
// A C++ program to solve eigenvalue problems.
#include<iostream>
#include<iomanip.h>
#include<fstream>
#include<string>
#include<math.h>
#include<cassert>
using namespace std;

const int dim=60;               //number of layers;
const double pi=3.14159;        //π value;
const double g=9.8;             //gravitational acceleration;
const double fi=pi*20/180.0;            // friction angle;
const double sita=pi*57.8/180.0;        //packing angle of kernels;
const double lo=797.57;                 //bulk density

typedef double emtrx[dim][dim];
typedef double mtrx[dim][3];
typedef double vec[dim];

void infunc(int n,ifstream &fin,mtrx &stiff,vec &mass);
```

```
void calfunc(int n,int n1,mtrx &stiff,vec &mass,vec &x,vec &evlu,emtrx &evct);
void psolv(int n,int &nj,int &count,mtrx &stiff,vec &mass,vec &x1,vec &x,vec &y1,vec &y,double
&lumda1,double &lumda2,vec &evlu,emtrx &evct);
void eqsolv(int n,mtrx &stiff,vec &y1,vec &x);
void masmul(int n,vec &mass,vec &x,vec &y);
double ldcal(int n,vec &x,vec &y1,vec &y);
void nvecy(int n,int nj,vec &mass,vec &x1,vec &y1,vec &x,vec &y,emtrx &evct);
void eigenv(int n,vec &x,vec &y);

int main()
{
    int n, n1;
    emtrx evct;
    mtrx stiff;
    vec mass, x, evlu;
    string iname;
    cout<<"enter input file name:"<<endl;
    getline(cin, iname);
    ifstream fin;
    fin.open(iname.data());
    fin>>n>>n1;
    infunc(n,fin,stiff,mass);
    calfunc(n,n1,stiff,mass,x,evlu,evct);
    for(int i=0;i<n;i++)
    {
       for(int j=0;j<n1;j++)
       {
         evct[j][i]=evct[j][i]/evct[j][n-1];
         cout<<evct[j][i]<<"   ";
```

```
        }
        cout<<endl;
    }
    return(0);
}

void infunc(int n,ifstream &fin,mtrx &stiff,vec &mass)
{
    double ke, stif, y0, le;
    fin>>ke>>y0;
    stif=2*ke*sin(sita)*sin(sita);
        stiff[0][0]=stif;
        stiff[0][1]=-stif;
        stiff[0][2]=0;
    for(int i=1; i<(n-1); i++)
    {
        stiff[i][0]=-stif;
        stiff[i][1]=2*stif;
        stiff[i][2]=-stif;
    };
        stiff[n-1][0]=0;
        stiff[n-1][1]=-stif;
        stiff[n-1][2]=2*stif;
    le=y0/n;
    for(int i=0;i<n;i++)
    {
        mass[i]=le*lo;
    }
    fin.close();
```

```
}

void calfunc(int n,int n1,mtrx &stiff,vec &mass,vec &x,vec &evlu,emtrx &evct)
{
  double lumda1=0, lumda2=0,f;
  vec x1, y1, y;
  for(int nj=0;nj<n1;nj++)
  {
   int count=0;
   if(nj==0)
   {
     for(int i=0;i<n;i++)
     {
        if(i==nj) x1[i]=1;
        else     x1[i]=0;
        y1[i]=mass[i]*x1[i];
     };
     psolv(n,nj,count,stiff,mass,x1,x,y1,y,lumda1,lumda2,evlu,evct);
//   for(int i=0;i<n;i++)
//   {
//      cout<<"x["<<i<<"]= "<<x[i]<<"     y["<<i<<"]=  "<<y[i]<<endl;
//   }
     f=(sqrt(lumda2))/2/pi;
     evlu[nj]=f;
     for(int i=0;i<n;i++)
     {
        evct[nj][i]=x[i];
     }
   }
```

```
else
{
  for(int i=0;i<n;i++)
  {
     if(i==nj) x1[i]=1;
     else     x1[i]=0;
     y1[i]=mass[i]*x1[i];
  };
  vec beta;
  for(int i1=0;i1<nj;i1++)
  {
     beta[i1]=0;
     for(int i2=0;i2<n;i2++)
     {
       beta[i1]=beta[i1]+evct[i1][i2]*mass[i2]*x1[i2];
     }
  }
  for(int i2=0;i2<n;i2++)
  {
     for(int i1=0;i1<nj;i1++)
     {
       x1[i2]=x1[i2]-beta[i1]*evct[i1][i2];
     }
     y1[i2]=mass[i2]*x1[i2];
  }
  psolv(n,nj,count,stiff,mass,x1,x,y1,y,lumda1,lumda2,evlu,evct);
  f=(sqrt(lumda2))/2/pi;
  evlu[nj]=f;
  for(int i=0;i<n;i++)
```

```
      {
         evct[nj][i]=x[i];
      }
    }
    cout<<"**********"<<endl;
    cout<<lumda1<<"    "<<lumda2<<endl;
    cout<<"count= "<<count<<"       f="<<f<<endl;
  }
}

void psolv(int n,int &nj,int &count,mtrx &stiff,vec &mass,vec &x1,vec
&x,vec &y1,vec &y,double &lumda1,double &lumda2,vec &evlu,emtrx &evct)
{
      double dif;
      eqsolv(n,stiff,y1,x);
      masmul(n,mass,x,y);
      count++;
      if(count==1)
      {
        lumda1=ldcal(n,x,y1,y);
        nvecy(n,nj,mass,x1,y1,x,y,evct);
        psolv(n,nj,count,stiff,mass,x1,x,y1,y,lumda1,lumda2,evlu,evct);
      }
      else
      {
         lumda2=ldcal(n,x,y1,y);
         dif=(lumda2-lumda1)/lumda2;
           cout<<"dif="<<dif<<endl;
         if(fabs(dif)<0.005||count>30)
```

```
        {
          eigenv(n,x,y);

        }
        else
        {
    lumda1=lumda2;
    nvecy(n,nj,mass,x1,y1,x,y,evct);
    psolv(n,nj,count,stiff,mass,x1,x,y1,y,lumda1,lumda2,evlu,evct);
        }
      }
}

void eqsolv(int n,mtrx &stiff,vec &y1,vec &x)
{
      vec tem;
      for(int i=0;i<n;i++)
      {
         tem[i]=y1[i];
      }
      for(int i=1;i<n;i++)
      {
         for(int j=0;j<i;j++)
         {
           tem[i]=tem[i]+y1[j];
         }
      }
      x[n-1]=tem[n-1]/stiff[0][0];
      for(int i=(n-2);i>-1;i--)
```

```
    {
        x[i]=(tem[i]+stiff[0][0]*x[i+1])/stiff[0][0];
    }
}

void masmul(int n,vec &mass,vec &x,vec &y)
{
    for(int i=0;i<n;i++)
    {
        y[i]=mass[i]*x[i];
    }
}

double ldcal(int n,vec &x,vec &y1,vec &y)
{
    double tem1=0;
    double tem2=0,tem;
    for(int i=0;i<n;i++)
    {
        tem1=tem1+x[i]*y1[i];
        tem2=tem2+x[i]*y[i];
    }
    tem=tem1/tem2;
    return(tem);
}

void nvecy(int n,int nj,vec &mass,vec &x1,vec &y1,vec &x,vec &y,emtrx
&evct)
{
```

```
double tem=0;
vec bta;
for(int i=0;i<n;i++)
{
    tem=tem+x[i]*x[i];
}
tem=sqrt(tem);
if(nj==0)
{
    for(int i=0;i<n;i++)
    {
        x1[i]=x[i]/tem;
        y1[i]=x1[i]*mass[i];
    }
}
else
{
    for(int i=0;i<n;i++)
    {
        x1[i]=x[i]/tem;
    }
    for(int i1=0;i1<nj;i1++)
    {
        bta[i1]=0;
        for(int i2=0;i2<n;i2++)
        {
            bta[i1]=bta[i1]+evct[i1][i2]*mass[i2]*x1[i2];
        }
    }
```

```
        for(int i2=0;i2<n;i2++)
        {
            for(int i1=0;i1<nj;i1++)
            {
                x1[i2]=x1[i2]-bta[i1]*evct[i1][i2];
                y1[i2]=x1[i2]*mass[i2];
            }
        }
        tem=0;
        for(int i=0;i<n;i++)
        {
            tem=tem+x1[i]*x1[i];
        }
        tem=sqrt(tem);
        for(int i=0;i<n;i++)
        {
          x1[i]=x1[i]/tem;
          y1[i]=x1[i]*mass[i];
        }
    }
}

void eigenv(int n,vec &x,vec &y)
{
    double tem=0;
    for(int i=0;i<n;i++)
    {
        tem=tem+x[i]*y[i];
    }
```

```
    tem=sqrt(tem);
    for(int i=0;i<n;i++)
    {
       x[i]=x[i]/tem;
    }
}
```

Appendix D. C++ CODE FOR OPTIMAL FREQUENCIES OF A BULK SOLIDS SYSTEM

```
// A C++ program to select the optimal frequencies for a bulk solids system.
#include<iostream>
#include<iomanip.h>
#include<fstream>
#include<string>
#include<math.h>
#include<cassert>
using namespace std;

const int dim=200;
const double pi=3.14159;
const double g=9.8;
const double fi=pi*25/180.0;
const double lo=568;

typedef double emtrx[dim][dim];
typedef double mtrx[dim][3];
typedef double vec[dim];

void infunc(int n,double &y0,ifstream &fin,mtrx &stiff,vec &mass);
```

```
void calfunc(int n,int n1,mtrx &stiff,vec &mass,vec &x,vec &evlu,emtrx
&evct);
void psolv(int n,int &nj,int &count,mtrx &stiff,vec &mass,vec &x1,vec
&x,vec &y1,vec &y,double &lumda1,double &lumda2,vec &evlu,emtrx &evct);
void eqsolv(int n,mtrx &stiff,vec &y1,vec &x);
void masmul(int n,vec &mass,vec &x,vec &y);
double ldcal(int n,vec &x,vec &y1,vec &y);
void nvecy(int n,int nj,vec &mass,vec &x1,vec &y1,vec &x,vec &y,emtrx
&evct);
void eigenv(int n,vec &x,vec &y);
void shape(int n,int n1,double &y0,emtrx &evct,vec &peak1, vec &peak2);
int main()
{
    int n, n1;
    double y0;
    emtrx evct;
    mtrx stiff;
    vec mass, x, evlu, peak1, peak2;
    string iname;
    cout<<"enter input file name:"<<endl;
    getline(cin, iname);
    ifstream fin;
    fin.open(iname.data());
    fin>>n>>n1;
    ofstream fout;
    fout.open("mash-eigen.dat");
    infunc(n,y0,fin,stiff,mass);
    calfunc(n,n1,stiff,mass,x,evlu,evct);
    shape(n,n1,y0,evct,peak1,peak2);
```

```
    for(int i1=0;i1<n1;i1++)
    {
     cout<<"f [ "<<i1<<" ] =  "<<evlu[i1]<<"    "<<endl;
     fout<<"f [ "<<i1<<" ] =  "<<evlu[i1]<<"    "<<endl;;
    }
    for(int i=0;i<n;i++)
    {
     int i1;
     i1=n-i-1;
     for(int j=0;j<n1;j++)
     {
       cout<<"ei["<<j<<"]["<<i<<"]="<<setw(9)<<evct[j][i1]<<"   ";
       fout<<"ei["<<j<<"]["<<i<<"]="<<setw(9)<<evct[j][i1]<<"   ";
     }
     cout<<endl;
     fout<<endl;
    }
    for(int i=0;i<n1;i++)
    {
     fout<<peak1[i]<<"      "<<peak2[i]<<endl;
    }
    cout<<"Sulotion has also been written to a data file: mash-eigen.dat"<<endl;
    fout.close();
    return(0);
}

void infunc(int n,double &y0,ifstream &fin,mtrx &stiff,vec &mass)
{
    double ke, stif, le;
```

```
    fin>>ke>>y0;
    stif=ke;
        stiff[0][0]=stif;
        stiff[0][1]=-stif;
        stiff[0][2]=0;
    for(int i=1; i<(n-1); i++)
    {
        stiff[i][0]=-stif;
        stiff[i][1]=2*stif;
        stiff[i][2]=-stif;
    };
        stiff[n-1][0]=0;
        stiff[n-1][1]=-stif;
        stiff[n-1][2]=2*stif;
    le=y0/n;
    for(int i=0;i<n;i++)
    {
        mass[i]=le*lo;
    }
    fin.close();
}

void calfunc(int n,int n1,mtrx &stiff,vec &mass,vec &x,vec &evlu,emtrx &evct)
{
  double lumda1=0, lumda2=0,f;
  vec x1, y1, y;
  for(int nj=0;nj<n1;nj++)
  {
   int count=0;
```

```
    if(nj==0)
    {
      for(int i=0;i<n;i++)
      {
         if(i==nj) x1[i]=1;
         else     x1[i]=0;
         y1[i]=mass[i]*x1[i];
      };
      psolv(n,nj,count,stiff,mass,x1,x,y1,y,lumda1,lumda2,evlu,evct);
//    for(int i=0;i<n;i++)
//    {
//       cout<<"x["<<i<<"]= "<<x[i]<<"    y["<<i<<"]=  "<<y[i]<<endl;
//    }
      f=(sqrt(lumda2))/2/pi;
      evlu[nj]=f;
      for(int i=0;i<n;i++)
      {
         evct[nj][i]=x[i];
      }
    }
    else
    {
      for(int i=0;i<n;i++)
      {
         if(i==nj) x1[i]=1;
         else     x1[i]=0;
         y1[i]=mass[i]*x1[i];
      };
      vec beta;
```

```
    for(int i1=0;i1<nj;i1++)
    {
       beta[i1]=0;
       for(int i2=0;i2<n;i2++)
       {
         beta[i1]=beta[i1]+evct[i1][i2]*mass[i2]*x1[i2];
       }
    }
    for(int i2=0;i2<n;i2++)
    {
       for(int i1=0;i1<nj;i1++)
       {
         x1[i2]=x1[i2]-beta[i1]*evct[i1][i2];
       }
       y1[i2]=mass[i2]*x1[i2];
    }
    psolv(n,nj,count,stiff,mass,x1,x,y1,y,lumda1,lumda2,evlu,evct);
    f=(sqrt(lumda2))/2/pi;
    evlu[nj]=f;
    for(int i=0;i<n;i++)
    {
       evct[nj][i]=x[i];
    }
  }
  cout<<"**********"<<endl;
  cout<<lumda1<<"    "<<lumda2<<endl;
  cout<<"count= "<<count<<"       f="<<f<<endl;
 }
}
```

```
void psolv(int n,int &nj,int &count,mtrx &stiff,vec &mass,vec &x1,vec
&x,vec &y1,vec &y,double &lumda1,double &lumda2,vec &evlu,emtrx &evct)
{
    double dif;
    eqsolv(n,stiff,y1,x);
    masmul(n,mass,x,y);
    count++;
    if(count==1)
    {
      lumda1=ldcal(n,x,y1,y);
      nvecy(n,nj,mass,x1,y1,x,y,evct);
      psolv(n,nj,count,stiff,mass,x1,x,y1,y,lumda1,lumda2,evlu,evct);
    }
    else
    {
       lumda2=ldcal(n,x,y1,y);
       dif=(lumda2-lumda1)/lumda2;
         cout<<"dif="<<dif<<endl;
       if(fabs(dif)<0.000000005||count>1000)
       {
         eigenv(n,x,y);
       }
       else
       {
  lumda1=lumda2;
  nvecy(n,nj,mass,x1,y1,x,y,evct);
  psolv(n,nj,count,stiff,mass,x1,x,y1,y,lumda1,lumda2,evlu,evct);
       }
    }
```

```
}

void eqsolv(int n,mtrx &stiff,vec &y1,vec &x)
{
    vec tem;
    for(int i=0;i<n;i++)
    {
       tem[i]=y1[i];
    }
    for(int i=1;i<n;i++)
    {
       for(int j=0;j<i;j++)
       {
         tem[i]=tem[i]+y1[j];
       }
    }
    x[n-1]=tem[n-1]/stiff[0][0];
    for(int i=(n-2);i>-1;i--)
    {
       x[i]=(tem[i]+stiff[0][0]*x[i+1])/stiff[0][0];
    }
}

void masmul(int n,vec &mass,vec &x,vec &y)
{
    for(int i=0;i<n;i++)
    {
       y[i]=mass[i]*x[i];
    }
```

```
}

double ldcal(int n,vec &x,vec &y1,vec &y)
{
    double tem1=0;
    double tem2=0,tem;
    for(int i=0;i<n;i++)
    {
        tem1=tem1+x[i]*y1[i];
        tem2=tem2+x[i]*y[i];
    }
    tem=tem1/tem2;
    return(tem);
}

void nvecy(int n,int nj,vec &mass,vec &x1,vec &y1,vec &x,vec &y,emtrx &evct)
{
    double tem=0;
    vec bta;
    for(int i=0;i<n;i++)
    {
        tem=tem+x[i]*x[i];
    }
    tem=sqrt(tem);
    if(nj==0)
    {
        for(int i=0;i<n;i++)
        {
            x1[i]=x[i]/tem;
```

```
        y1[i]=x1[i]*mass[i];
    }
}
else
{
    for(int i=0;i<n;i++)
    {
        x1[i]=x[i]/tem;
    }
    for(int i1=0;i1<nj;i1++)
    {
        bta[i1]=0;
        for(int i2=0;i2<n;i2++)
        {
            bta[i1]=bta[i1]+evct[i1][i2]*mass[i2]*x1[i2];
        }
    }
    for(int i2=0;i2<n;i2++)
    {
        for(int i1=0;i1<nj;i1++)
        {
            x1[i2]=x1[i2]-bta[i1]*evct[i1][i2];
            y1[i2]=x1[i2]*mass[i2];
        }
    }
    tem=0;
    for(int i=0;i<n;i++)
    {
        tem=tem+x1[i]*x1[i];
```

```
        }
        tem=sqrt(tem);
        for(int i=0;i<n;i++)
        {
          x1[i]=x1[i]/tem;
          y1[i]=x1[i]*mass[i];
        }
    }
}

void eigenv(int n,vec &x,vec &y)
{
    double tem=0;
    for(int i=0;i<n;i++)
    {
       tem=tem+x[i]*y[i];
    }
    tem=sqrt(tem);
    for(int i=0;i<n;i++)
    {
       x[i]=x[i]/tem;
    }
}

void shape(int n,int n1,double &y0,emtrx &evct,vec &peak1, vec &peak2)
{
    for(int i=0;i<n1;i++)
    {
     double tem;
```

```
 tem=evct[i][0];
 for(int j=0;j<n;j++)
 {
   if(fabs(tem)<fabs(evct[i][j]))
   {
     tem=fabs(evct[i][j]);
   }
   else ;
 }
 for(int j=0;j<n;j++)
 {
   evct[i][j]=evct[i][j]/tem;
 }
}
for(int i=0;i<n1;i++)
{
 peak1[i]=0;
 peak2[i]=0;
 for(int j=n-1;j>1;j--)
 {
   if(j==n-1 && fabs(evct[i][j])>fabs(evct[i][j-1]))
   peak1[i]=(n-j)*y0/n;
   else if(fabs(evct[i][j])<fabs(evct[i][j-1]) && fabs(evct[i][j-1])>fabs(evct[i][j-2]) )
   {
      if(peak1[i]==0) peak1[i]=(n-j+1)*y0/n;
      else if(peak2[i]==0) peak2[i]=(n-j+1)*y0/n;
      else ;
   }
   else if(j==2 && fabs(evct[i][j-1])<fabs(evct[i][j-2]))
```

```
        {
          if(peak1[i]==0) peak1[i]=(n-j+2)*y0/n;
          else if(peak2[i]==0) peak2[i]=(n-j+2)*y0/n;
        }
        else ;
      }
      if(peak2[i]==0) peak2[i]=peak1[i];
      else ;
    }
}
```